Final Report

Project UXO-1387

"Seismic Imaging of UXO-Contaminated Underwater Sites"

Roland Gritto[1,2], Valeri Korneev[1], Kurt Nihei[1], Lane Johnson[1]

[1]Lawrence Berkeley National Laboratory
and
[2]University of California Berkeley
Department of Environmental Sciences and Engineering

This report was prepared under contract to the Department of Defense Strategic Environmental Research and Development Program (SERDP). The publication of this report does not indicate endorsement by the Department of Defense, nor should the contents be construed as reflecting the official policy or position of the Department of Defense. Reference herein to any specific commercial product, process, or service by trade name, trademark, manufacturer, or otherwise, does not necessarily constitute or imply its endorsement, recommendation, or favoring by the Department of Defense.

Summary

Two- and three-dimensional numerical modeling was conducted to evaluate the performance of source-receiver arrays to "detect" and "locate" UXO in littoral environments. While the 2-D investigations were based on finite difference (FD) modeling, the 3-D study used an analytical solution for the scattering of elastic waves by spherical objects to model the interaction of waves with UXO. The forward modeling or "detection" phase generated seismic data that reveal the presence of UXO in the subsurface. The inverse modeling or "location" phase was based on 2-D and 3-D migration techniques applied to the data generated during the forward modeling. The model parameters were taken from measurements in coastal areas with typical bay mud and from examples in the literature. Seismic arrays are well suited to focus energy by steering the elements of the array to any point of interest in the medium. This principle also applies to seismic waves that are backscattered by buried UXO. The power of the array is particularly evident in strong noise conditions, when the signal-to-noise ratio is too low to observe the scattered signal on the seismograms. Using a seismic array, it was possible to detect and locate UXO with a reliability similar to noise-free situations. Proud objects are problematic to detect, because their scattered waves interfere with the reflections of the seafloor interface. However, it was found that as long as the impedance contrast between the surrounding medium and the UXO is larger than the impedance contrast across the interface, the UXO reflection dominates the seafloor reflection. When the UXO was positioned within 3-6 wavelengths of the incident signal from the source array, the resolution was good enough to determine the dimensions of the UXO from the scattered waves. Beyond this distance this distinction decreased gradually, while the location and the center of the UXO were still determined reliably. The location and the dimensions of two adjacent UXO were resolved down to a separation of 1/3 of the dominant wavelength of the incident wave, at which time interference effects began to appear. In the investigated cases, the ability to locate a UXO was independent on the use of a model with a rippled or a flat seafloor, as long as the array was located above the UXO. Even though a flat interface was used during the inversion step, the correct parameters (wavelength and peak-to-trough amplitude) of the seafloor interface were successfully determined in these cases. An investigation to find the correct migration velocity to locate UXO in the sediments revealed that the migrated image with the most coherent amplitude signature is correlated to the correct velocity gradient, such that this important subsurface parameter can be determined during the migration step. At the same time, a range of velocity gradients centered about the correct velocity model produced comparable results. The correct design of 2-D receiver arrays is important to suppress waves that otherwise interfere with the signal of interest. However, a well-designed array is capable of detecting and locating UXO in space even under strong noise conditions. Scattering of elastic waves by UXO generates mode conversion and radiates energy in complicated patterns. These patterns, although complicated, are the signature of the scattering objects and can be used for discrimination purposes. Because P-to-S scattering is stronger than P-to-P scattering in most cases, S-wave can provide important complementary information that can help to discriminate the nature of the UXO. Therefore, it should be investigated how S-waves can be excited and propagated in the seafloor sediments. The D.O.R.T. method could provide an important tool for UXO

detection, as it allows to focus energy on selected objects in the medium. In the investigated example, it was possible to steer the array to focus energy on two isolated scatterers of different strength.

Introduction

Detection and Location of UXO in Littoral Environments

In recent years, the evolution in hydrocarbon exploration from two- to three-dimensional seismic methods has resulted in improved resolution and better definition of the subsurface geological structure and prospects. These methods were developed to overcome the complicated structure of some areas where tectonic features (i.e., faults, fractures, salt domes) adversely affect seismic wave propagation through strong scattering and attenuation. Although the heterogeneity of the media and the experimental geometries encountered in littoral UXO detection are less complex than those of geologic crustal-scale investigations, the marine environment still comprises a high degree of complexity considering the short wavelengths of the seismic waves needed to yield sufficient resolution. The rugosity of the seafloor determines the coupling and the coherency of the seismic wavefield as it propagates into and out of the sediments, and therefore, the signal-to-noise ratio of the backscattered energy by the UXO. However, seafloor rugosity can scatter coherent energy into the sediments at angles larger than the critical angle. Biologic activity in the upper parts of the sediments may cause anaerobic conditions producing gas pockets that attenuate the acoustic signal and constrain the maximum penetration of the waves. If free gas is present in the sediments, it may produce anelastic attenuation particularly for the high frequency components of the seismic signal. Therefore, research is needed to investigate whether arrays of seismic sources and receivers can be used to increase seismic energy levels radiated into the seafloor and how the signal-to-noise ratio of the back-scattered seismic energy can be improved by beamforming and focusing the energy onto the UXO target. The current project addressed these questions based on numerical modeling, where seismic arrays were deployed in the water column and along the seafloor to focus beams of energy into seafloor sediments to improve the signal-to-noise ratio of seismic waves backscattered by UXO and to lower the threshold of the detection method.

The detection of the presence of UXO is followed by their location in the medium, which requires knowledge about the velocities in the seafloor sediments. The determination of the location was also addressed in this project, where a migration approach is employed which simultaneously estimates seafloor rugosity and the velocity gradient of the sediments, while locating UXO in space.

This report summarizes the accomplishments of the SERDP seed project "Seismic Imaging of UXO-Contaminated Underwater Sites" over the six months duration of the project including Tasks 1-3 and 5 (with Task 4 being the interim report). The current research is intended as a first stage of a more extended project to detect, locate, and discriminate UXO in littoral environments based on seismic imaging methods. While this seed project addresses the problem of improving UXO detection using array techniques numerically, future research, if funded, will be directed towards physical modeling of the detection and location and in particular the discrimination of UXO based on seismic

scattering techniques. Recent developments to determine the location and the elastic properties of strong scatterers using scattered seismic waves (Gritto 1995, Gritto et al., 1999) offer the right approach to discriminate UXO, because the underlying principle of these developments can be directly applied to the UXO problem.

Task 1: Determination of Modeling Parameters at Mare Island, CA

The first task was concerned with the determination of physical parameters typical of littoral areas where UXO contamination is expected. These parameters are needed to build numerical models as a basis for finite-difference and analytical modeling, which are the primary tasks of the current SEED project. The parameters were chosen to be representative for a typical clean-up site (BRAC site) as in the case of the formal naval shipyard at Mare Island, Vallejo, CA. This site contains on- and off-shore UXO contamination and has undergone several clean-up cycles in the past (mainly on-shore). The physical parameters included seismic velocities and attenuation, mud densities and porosities, and sedimentary thickness to bedrock. In addition, the field parameters were complemented by estimates taken from the literature (Hamilton, 1971, 1972, 1976; Stoll, 1985; Kibblewhite, 1989) that are typical for these types of bay mud (clayey silts, and silty clays). The physical parameters were determined as:

<u>Salt Water Parameters</u>

P-wave velocity:	1510 m/s
S-wave velocity:	0 m/s
Density :	$1.03 \cdot 10^3$ kg/cm^3
Water depth:	1-3 m

<u>Bay Mud Parameters</u>

P-wave velocity:	1520 m/s – 1600 m/s (0-5 m depth)
S-wave velocity:	100 m/s – 150 m/s (0-5 m depth)
Wet Bulk Density:	$1.4 \cdot 10^3$ kg/cm^3
Porosity :	70 %
Sedimentary thickness:	> 10 m
Attenuation α:	0.2 dB/kHz/m
Quality factor Q:	88

These physical parameters were subsequently used to build numerical models for wave propagation simulations using FD and analytical modeling.

Task 2: 2-D Modeling: Analysis of Single Source Receiver Pairs

The second task was concerned with numerical FD modeling of single source and receiver combinations to investigate the amount of energy reflected and transmitted at the water-seafloor interface and scattered by the UXO. This investigation was carried out using 2-D FD models based on the physical parameters determined in Task 1. A schematic of the model is shown in Figure 1. The dimensions of the model were 6 m by 6

m with a water- and sediment depth of 3 m each. Because the depth to bedrock was greater than 10 m at the Mare Island test site, the sediment/bedrock interface was not modeled, as the associated reflected waves would fall far outside the time interval of interest for reflections off the UXO. The parameters of the FD model are summarized in Table 1.

Table1: Finite Difference Modeling Parameters

	Salt Water Parameters	Bay Mud Parameters	UXO Parameters	Numerical Parameters
P-wave velocity [m/s]	1510	1520-1600	6568	
S-wave velocity [m/s]	0	0	3149	
Density [kg/m^3]	$1.03 \cdot 10^3$	$1.4 \cdot 10^3$	$2.7 \cdot 10^3$	
Depth [m]	3.0	3.0		
Quality Factor	∞	88	∞	
Length [m]	3.0	3.0		
Dimensions (x,z) [m]			0.3 by 0.1	
Node Spacing [m]				0.01
Number of Nodes (x,z)				600 by 600
Sample Interval [s]				10^{-5}
Source Frequency [Hz]				$5 \cdot 10^{+3}$

Various source signals and frequencies were investigated with the final signal being a Ricker wavelet (Gaussian derivative) with a central frequency of 5 kHz. The source frequency translates to a dominant wavelength of approximately λ_0=0.3 m for the P-wave in the bay sediments. Once the parameters were chosen, the FD code was tested for numerical stability to guarantee dispersion-free results. The single source-receiver experiment was intended to provide a baseline measurement for the reflection of seismic energy off the UXO and to evaluate the improvement using source-receiver arrays. A more detailed display of the velocity model including the locations of a single source, an array of receivers, and a UXO is presented in Figure 2. The source and receiver array are located at a water depth of 1m, while the UXO is located 1 m below the water/sediment interface. While the velocity in water is homogenous at v_p=1510 m/s, the sediment-velocity is modeled by a tangential gradient from 1520-1600 m/s. The receiver array in Figure 2 consists of 31 receiver elements with a separation of 0.1 m. The seismic traces recorded from a shot located at x=1.0m and z=1.0 m are shown in Figure 3. Three arrivals are visible representing in sequence of arrival time the direct propagating P-wave, the P-wave reflected off the water/sediment interface, and the P-wave scattered of the UXO. It can be seen that the amplitudes of the UXO-scattered phases and the interface reflections are comparable in amplitude and separated in time for this shot geometry. Therefore, it should be possible to migrate the location of the UXO in space.

However, for any given single source receiver pair, where the receiver is a pressure sensor, it is impossible to locate an object in space because of lack of directionality. In the present case, a migration of the signal recorded by the first receiver produced the results presented in Figure 4. In this case the migration was performed for a

depth range between 2.5 m and 6.0 m only. Although the migrated amplitudes stack up along ellipses that touch the interface as well as the UXO, the exact location of the UXO or the interface cannot be determined. Similar to the seismic section in Figure 3, both signals reveal comparable amplitudes after migration. Therefore, the introduction of multiple receivers (pressure sensors) is necessary to determine the location of the UXO, which will also improve the signal to noise ratio.

Task 3: 2-D Modeling: Analysis of Beamforming Techniques for 1-D Source-Receiver Arrays

Source-Receiver Array Located in Water

The receiver array in Figure 2 consisted of 31 sensors, which can be used to steer a beam of recorded energy at any point in the medium. To illustrate this point the energy of a point pressure source located in a homogeneous medium at x=2.5 m and z=4.0 m is shown in Figure 5. It can be seen that the energy decays radially from the source. If this energy is recorded with the receiver array located above the source, the array can be steered to illuminate the source location. This is done by reversing the time delay recorded between traces of the original wavefield to focus energy onto the intended target. The result of the beamforming is presented in Figure 6. The focused energy beam is centered on the source location and the width is greatly reduced compared to the energy radiated from the single source. In the same way, the array can be steered to illuminate each point in the medium to improve the detection of UXO in the subsurface.

The use of a full array of sources and receivers is presented in the next example where 31 sources are co-located with the receiver array from the previous example. In the present case a total of 961 seismograms were recorded, which contained reflections off the water/sediment interface and off the UXO as presented in Figure 3. The velocity model used for the migration was the same as for the FD modeling. The travel times from the source and receiver locations to each point in the subsurface were calculated using a 2-D eikonal solver (Podvin and Lecompte, 1991). The migration included the computation of the travel times for each source/receiver combination to each point in the medium below the array followed by stacking the root mean square (rms) amplitude over a predefined window on the seismogram. The idea is that the amplitudes on the traces will stack constructively for locations in the medium that scattered energy, while they will stack destructively for locations that did not scatter energy. The resulting amplitude values are subsequently plotted as a function of location in the medium. The result of this migration is presented in Figure 7 for a depth range from 2.5 m to 6 m. A weak amplitude signature with values of 0.3 indicates the location of the water/sediment interface at 3 m depth. Although the reflections from the interface and the UXO revealed comparable amplitudes in Figure 3, the averaging over the whole receiver array enhanced the phases scattered by the UXO, because the migration approach enhances the stacked signals of point scatterers, while it averages the stacked signal from planar features. The result is a pronounced peak at the location of the UXO. The noise level of the migrated image is low, due to the high number of sources and receivers in the array. Two cross sections of the amplitude structure in Figure 7 are provided in Figure 8, where the amplitude is

shown as a function of distance and depth across the model. It can be seen that the maximum of the amplitude coincides with the center of the UXO in x-direction, while it coincides with the top of the UXO in z-direction. The latter is caused by the impedance contrast between the top of the UXO and the sediment, which produces the reflected seismic signal. In addition to the UXO signature in z-direction, the water/sediment interface is indicated by an amplitude level of 0.3 at 3 m depth. The focusing of the array produced a sharp seismic signature of the UXO and a high signal to noise ratio evident by the low background amplitude level, which quickly decreases with increasing distance from the UXO location.

In a natural environment there are numerous correlated and uncorrelated noise sources that have an adverse affect on the power and resolution of any detection algorithm. In the following example, the case of uncorrelated noise was examined, while correlated noise sources were treated in a later section. To test the stability of the inversion algorithm in the presence of noise, varying degrees of uncorrelated Gaussian distributed noise were added to the seismic waveforms shown in Figure 3. A waveform example with a noise level of 50% is presented in Figure 9. To compute a noise level that is related to the seismic UXO signal rather than the water/sediment interface reflections, the rms value of each seismic signal scattered by the UXO is computed as a basis for the noise. Therefore, the absolute noise level of each trace is distinct, based on the strength of the amplitudes scattered by the UXO as evident in Figure 9. The 50% noise level is high enough to obscure most of the scattered UXO signal between 4.0 ms and 4.5 ms on the seismogram (compare to Figure 3). This extreme case was chosen to test the performance of the source-receiver array. The result of the migration is presented in Figure 10 and should be compared to the noise-free situation in Figure 7. Although the noise level of the background is somewhat elevated, it is evident that the location of the UXO is correctly determined and the outline of the amplitude structure is comparable to that in Figure 7. At the same time the water/sediment interface is correctly located with an amplitude level equivalent to the noise-free case. The cross sections through the image reveal the elevated noise background in Figure 11, which is about 4% of the amplitude maximum. At the same time it can be seen that the shape of the amplitude structure in both cross sections is comparable to the noise-free case in Figure 8. This example illuminates the power of source-receiver arrays to stack coherent signals constructively while suppressing uncorrelated noise at the same time. This result is promising for UXO location in littoral environments that exhibit a lot of uncorrelated noise.

Proud Objects

The detection and localization of proud objects is an important part of UXO cleanup efforts, when objects are only partly covered by sediments on the seafloor. In the last section, it was shown that the seafloor interface reflects seismic waves that are recorded and subsequently migrated during the location step. The result is an amplitude anomaly along the water/sediment interface. Therefore, it is important to determine how well proud objects can be detected and located in the presence of the seafloor interface. To address this question, the FD model from the previous example was used with the exception of the UXO positioned along the seafloor interface partly covered by

sediments, as indicated in Figure 12. The problem with this geometry is that reflections off the seafloor interface that are in close proximity to the UXO interfere with UXO reflections on the seismogram. A shot gather of waveforms generated by the source at x=1 m and z=1 m is shown in Figure 13. Three wave groups consisting of the direct wave, the seafloor reflections, and the UXO reflections are visible for near offset receivers (i.e., trace numbers 1-15). For far offsets the latter arrivals interfere and merge to a single pulse, which cannot be separated during the migration step. The result of the migration is presented in Figure 14. The seafloor reflection is apparent below the array with an average amplitude value of 0.2, which decays towards the edges of the array. The UXO reveals the strongest signal centered on the interface and is easily detectable over the seafloor reflection. In comparison to Figure 7, however, it can be seen that the noise level below the amplitude structure is slightly elevated. The details of the amplitude structure are better revealed in the cross sections in Figure 15. The maximum of the UXO amplitude structure coincides with the center of the UXO as seen in Figure 15a. In contrast to the results of a buried UXO (Figure 8), where the interface was indicated by an isolated feature in z-direction, the signature of the interface in this case is more easily recognized in x-direction, where it interferes with the UXO signature and slowly decays with increasing distance from the UXO, until it reaches background noise levels outside the bounds of the array. The vertical cross section in Figure 15b reveals that the amplitude maximum is slightly shifted below the top edge of the UXO, which is caused by interference with the interface reflection. This example indicates that proud objects can be detected and located using seismic arrays, because the migration algorithm favors point scatterers over planar reflections, and the elements of the source-receiver array amplify the constructive interference during the stacking of the UXO scattered phases. In general, it can be stated that the detection of proud objects is feasible for the tested geometries as long as long as the contrast in elastic properties between the UXO and the surrounding medium is stronger than the contrast between water and the seafloor sediments.

Source-Receiver Array Located on Seafloor

In order to obtain higher resolution images of the objects under investigation, the source-receiver array was placed on the seafloor to shorten the distance between the UXO and the array. In this case, the receivers consist of three-component motion- rather than pressure sensors, which simplifies the discrimination effort of the UXO. However, in the current study, where the emphasis was on detection rather than discrimination, we concentrated on the vertical component of the recorded wavefield. A seafloor array with dimensions identical to those used in the last section is shown in Figure 16, where the location of the UXO is kept the same. The wavefield excited by the source located at x=1.0 m and z=1.0 m is presented in Figure 17. Two arrivals can be distinguished, which are the direct P-wave and the waves scattered by the UXO. It can be seen that the scattered waves are composed of several arrivals, which include phases reflected off the top of the UXO, followed by phases that reverberate internally within the UXO, and finally waves that are multiple reflected between the UXO and the water/sediment interface. The migration of these wavefields produced a strong amplitude maximum

presented in Figure 18. Compared to the previous results the maximum is comprised of two peaks located towards the top edges of the UXO, which act as point scatterers reflecting the most energy. This feature is better resolved in the cross sections of the amplitude structure presented in Figure 19. It can be seen that the two maximums develop near the edges of the UXO, denoted by the dashed lines in Figure 19a. The vertical cross section in Figure 19b indicates that the maximum of the amplitude coincides with the top of the UXO as previously seen in Figure 8. The results of this example indicate that it is possible to determine the dimensions of the UXO if it is located within 3-6 wavelengths of the incident wave from the array. This situation can be achieved by placing the source-receiver array on the seafloor.

Considering the improved resolution of the seafloor array, capable of detecting the edges of UXO under the current conditions, it is of interest to evaluate the case of two UXO in close proximity and to investigate possible interference effects. Such a situation is presented in Figure 20, where an additional (green colored) UXO with the same dimensions but different orientation is located at a distance of 0.1 m from the first. The resulting scattered phases show a more complicated pattern and some interference is visible on traces 15 to 20 in Figure 21. The interference is also evident in the migrated amplitude image shown in Figure 22. Two partially merged amplitude structures are visible above the UXO, with the vertically oriented UXO producing the weaker response, while the background noise is slightly elevated over the single UXO case (compare to Figure 18). To evaluate the amplitude maximums more closely, three cross sections were computed for this case. The cross section in x-direction is shown in Figure 23a, while two cross sections traversing each UXO in z-direction are presented in Figures 19b,c. The color-coding of the dashed lines is intended to better cross-reference the UXO between figures. The amplitude cross section exemplifies the interference between the seismic signals. While the amplitudes scattered by (black colored) UXO 1 are generally stronger than those scattered by (green colored) UXO 2, the close proximity between them caused the scattered phases to interfere, producing reduced amplitude peaks for both UXO along the edges facing each other. Considering that the dominant wavelength of the incident wave is $\lambda_0 = 0.3$ m, this case might approach the limit of resolution in separating the two closely positioned UXO. The cross sections in z-direction support earlier findings. The maximum amplitude related to the horizontally oriented (black colored) UXO 1 in Figure 23b coincides with the top of the UXO as expected. However, interference between the two UXO caused the amplitude peak related to the vertically oriented (green colored) UXO 2 to appear just below its top (Figure 23c).

Rippled Seafloor and Free Surface Effects

In most cases the seafloor is not flat as modeled in the previous examples but consists of a sinusoidal profile caused by continuous wave action. However, it may be difficult to determine the sinusoidal amplitude and wavelength in field applications and thus it is important to determine the effect of these parameters on imaging results. To address this question, finite difference computations were performed based on the model presented in Figure 24. This model is similar to the one used before, except for a sinusoidal water/sediment interface with an amplitude of 0.04 m and a wavelength of

0.75 m (Lopes et al., 2003). Two models were computed, one with and the other without a free surface boundary condition for the water surface. A source gather of the model run without the free surface condition is presented in Figure 25. As previously seen, the three phases are the direct wave, the interface reflection, and the waves scattered by the UXO. An interesting observation about the interface reflections is the focusing and de-focusing effect visible throughout the traces. This is caused by the sinusoidal nature of the interface that focuses the reflected amplitudes into the array from some troughs on the interface while it de-focuses the amplitudes from others. When the free surface boundary condition is included in the modeling, the recorded waveforms take on the form presented in Figure 26. It is evident that the reflection off the water surface has become the dominant arrival on the seismogram. The effects of these wave phenomena on the migrated image will be shown in the next section.

The migration of the seismic waveforms was based on a velocity model with a flat water/sediment interface, because it is assumed that the amplitude and the wavelength of the sinusoidal interface are not known a priori. When the migrated area included the region in the vicinity below the seismic array (i.e., the migration is performed over a depth range between 1.5m and 6.0 m) a mirror image of the water surface appeared as the largest feature on the amplitude map at 2 m depth in Figure 27. This large anomaly suppresses the signature of the interface and the UXO as indicated in Figure 28, which shows the cross sections in x- and z-direction. It can be seen that the water surface signature is about twice as strong as that of the UXO. However, the geometry of the experiment prevented that multiples of the free surface reflection interfered with UXO scattered phases on the seismograms in Figure 26. In this case, the desired waveforms can be either separated in time on the seismograms, or the region where the free surface reflection appeared can be omitted during the migration procedure. In the latter case the phases stack destructively and will not be detectable elsewhere in the migration image. The result is shown in Figure 29, where the migration was limited to a depth greater than 2.5 m. It can be seen that the strongest amplitudes are now associated with the UXO signature. A closer look at the interface signature in Figure 29 reveals that it is discontinues towards the outer limits of the source-receiver array depending on whether the peaks and troughs reflect the signal back into the array or outside of its limits. The cross sections in Figure 30 show the improvement over the results in Figure 28, where the amplitude associated with the UXO becomes the dominant features again. Because factors like water depth, speed of sound in water, and the expected depth range of UXO in sediments can be estimated well enough prior to most experiments, the source-receiver array can be positioned such that interference of water surface reflection multiples with UXO reflections will be minimized. This is one example of how to avoid strong coherent noise during the migration process.

Although the migration was based on a velocity model with a flat seafloor, the result shows a correctly located interface that follows the sinusoidal character of the original boundary. The reason for this is the location of the source-receiver array straight above the interface. The near vertical raypaths, associated with the propagating waves, are very similar for the case of a flat or sinusoidal interface, such that travel time differences are negligible. However, this situation does not apply in the case of side-scan sonar (for example), because the associated rays encounter the interface at very large incident angles (measured from the vertical) and thus refract into the seafloor in the

presence of a rippled interface, while they reflect back into the water for a flat surface. The fact that the migration yields the correct amplitude and wavelength of the interface and the correct location of the UXO despite the a priori assumption of a flat bottom has important consequences for the characterization of the UXO. With the obtained information of the actual interface the velocity model can be refined and the discrimination of the UXO, which depends more on an accurate velocity model, becomes more reliable. However, the discrimination is not part of the current project.

Search for Correct Velocity Gradient

The previous investigations were based on the use of the same velocity model for FD modeling and migration, with the exception of the sinusoidal model in the last section. The intention was to determine how beamforming can improve the energy radiation into the subsurface and how it can increase the resolution of the location process. Using a source-receiver array the velocity in the water can be estimated as well as in the top sediments if the array is lowered onto the seafloor. However, the velocity-depth profile of the sediments is generally not known, and therefore, it is of interest to investigate whether the velocity of the sediments can be estimated during the migration process.

The velocity model used throughout this project was based on a tangential gradient, which was found as a good representation of the velocity increase in the shallow subsurface in many geophysical applications. The current velocity gradient is shown in Figure 31. For an object located in the shallow subsurface small deviations from the correct velocity function are not too detrimental during the migration if the image is averaged over many sources and receivers of a seismic array. Thus, to increase the sensitivity of the migration on the velocity model, a UXO was placed in the sediments 2.5 m below the seafloor to increase the propagation distance of the waves between the array and the UXO. The geometry of this case is given in Figure 32, which shows the inversion result of the migration using the correct velocity gradient. If the correct velocity model is used, the scattered phases are stacked constructively and correctly located during migration. Any deviation from the correct velocity model will produce incorrect shifts of the waveforms resulting in destructive interference during stacking and a reduced and spread amplitude image in space. Therefore, the amplitude of the UXO signature was used as a measure to determine the correct velocity gradient during migration. A total of 26 different velocity gradients were tested ranging from 1420 m/s to 1740 m/s as shown in Figure 33, where the correct gradient is indicated in red. For each gradient a separate migration was performed and the maximum of the UXO signature determined. The result is shown in Figure 34, where the maximum amplitude of each UXO signature is plotted as a function of velocity. The velocities represent the mean values of each gradient, while the dashed line indicates the mean velocity corresponding to the correct gradient. It can be seen that the amplitude maximum coincides with the correct velocity function as the migration produces the strongest amplitude image. However, it is also evident that the maximum is broad and that comparable high amplitude values were obtained for a range of velocities. This indicates that the migration process will produce similar, equally good, results even if the correct velocity gradient is

not precisely known. It should be kept in mind that this investigation was carried out for a UXO located at a sediment depth of 2.5 m, while in the majority of cases UXO are expected to be located at shallower depths where the influence of the correct velocity gradient is even less pronounced. This result seems promising for the location of UXO in shallow marine environments using seismic source-receiver arrays. The fact that the correct velocity gradient can be estimated during the migration process has been utilized in hydrocarbon exploration for many decades. The shallow depth range of UXO-contamination allows a more detailed analysis of the seafloor sediments. It is possible for example, to estimate the correct velocity gradient by burying an object in a representative area (without the presence of UXO) and calibrating the migration by producing the sharpest amplitude image that correlates with the (known) location of the target when the correct velocity gradient is used.

Task 5: 3-D Modeling: Analysis of Beamforming Techniques for 2-D and 1-D Source-Receiver Arrays

The 2-D modeling performed in Tasks 2 and 3 to investigate the kinematics and dynamics of UXO detection and location with seismic arrays yielded interesting results regarding the resolution and limitations of the approach and new ways to estimate subsurface parameters. However, the results were valid in 2-D only, while the actual location of UXO cannot be determined with a 1-D source-receiver geometry without additional information. The problem of UXO location in 3-D space requires the use of 2-D arrays to determine the location in the 3rd dimension. To investigate this concept, 3-D analytical modeling was chosen over 3-D FD modeling, because the numerical time requirements are much less for analytical methods. The employed method is based on the scattering of elastic waves by spherical objects (Korneev and Johnson, 1993a, 1993b) and is well suited for UXO applications as it is valid for all frequencies and contains near- and far-field terms, The elastic properties of the model are combined in Table 2. The analytical modeling includes the treatment of both P- and S-waves, because the numerical speed allows the calculation of the effects of both phases. In contrast, 2-D FD calculations would have been prohibitively expensive numerically, because of the fine node spacing required for the short wavelengths of S-waves. Although it is not clear whether S-waves can be propagated in shallow seafloor sediments, they will nevertheless be included in these simulations, to determine their usefulness to the localization and eventually to the discrimination problem. The frequencies of the source pulse were f_0= 5kHz and 15 kHz.

Table2: Analytical Modeling Parameters

	Bay Mud Parameters	UXO Parameters	Numerical Parameters
P-wave velocity [m/s]	1530	6568	
S-wave velocity [m/s]	120	3149	
Density [kg/m^3]	$1.4 \cdot 10^{+3}$	$2.7 \cdot 10^{+3}$	
Depth [m]	3.0		
Length [m]	3.0		
Diameter [m]		0.3	
Node Spacing in Migration [m]			0.01
Sample Interval [s]			10^{-5}
Source Frequency [Hz]			$5 \cdot 10^{+3}$, $15 \cdot 10^{+3}$

A schematic of the 3-D model is shown in Figure 35, where a cubic model of 6 m length is divided into a 3 m water layer above a 3m thick sedimentary layer. Thus the model is an extension of the 2-D FD model in the 3rd dimension. Three spherical UXO were placed in the subsurface along the x-z plane at y= 3 m and along the y-z plane at x= 3 m. The locations of the UXO are (x_1= 3 m, y_1= 3 m, z_1= 4 m), (x_2= 4 m, y_2= 3 m, z_2= 4.5 m), and (x_1= 3 m, y_1= 2.5 m, z_1= 5 m) as indicated in Figure 35. A 2-D array of 35 sources and 29 receivers is placed on the seafloor covering the plane above the UXO. The layout of the seismic array is more closely studied in the next section.

Seismic Array Response

The 2-D array consists of 35 regular spaced sources and 29 receivers that are arranged as indicated in Figure 36. The spacing of the receivers depends on the wavelengths of the recorded waves. As such, the spacing is a function of the velocity of the medium directly below the array, which governs the wavelength of the incident wave. The receivers need to be arranged to accommodate both, the shortest wavelengths to prevent aliasing and the largest wavelengths to be able to still focus the array on selected targets. While spacing is important, the location of the receivers relative to each other is equally important, because focusing the array in a specific directions should result in an interference-free response. This concept is explained in Figure 37, where the array response of the current receiver geometry is presented for the incidence of a plane wave with a frequency of 1 kHz. The plot shows the array response as a function of incident angles i_x and i_y in x- and y-direction, respectively. For the case of focussing in vertical direction (i.e, the array is sensitive to waves propagating in vertical direction), the highest sensitivity of the array is at 0° as expected. Furthermore, no other side lobes larger than 20% of the maximum are visible at other angles in the response plot. This indicates that waves, incident from other than the vertical direction, will be suppressed and won't interfere with the detection of vertically propagating waves. If the focus of the array is in a different direction (i.e., the reflected waves off UXO located off-center from the array should be recorded) the same principle applies. Figure 38 reveals the array response when

the array is focused at angles of –35° in x- and y-direction (i.e, the focus is towards the left quadrant in Figure 36). It can be seen that the response pattern is slightly changed, with the main lobe at i_x = –35° and i_y = –35°, but the side lobes are still small in amplitude relative to the main lobe. Therefore, waves propagating from other directions to the array won't interfere with the focus of the array on a target at i_x = –35° and i_y = –35°. The suppression of side lobes is an important aspect during the design stage of any array and needs to be carefully evaluated before the array can be used for data acquisition.

3-D Imaging of UXO with 5 kHz Data

After the array was tested, 3-D analytical modeling was performed to investigate the detection and localization of UXO in three dimensions. Because the geometry of the array is not as evenly spaced as in the 2-D case, the move-out of phases on the seismograms appear more irregular. Figure 39 shows a seismogram section for a source located at x= 0 m, y= 3 m, and z= 3 m and a group of five receivers located at y= 3 m between x= 0 m and 6 m. The two wave groups on the seismogram are the P- and S-waves reflected by the UXO. The seismogram represents the z-component of the particle velocity, which excludes the direct waves for the current geometry, where sources and receivers are located at the same elevation. The three pulses for each wave group represent reflections from the three UXO at depth. The first trace did not record S-wave energy, because source and receiver were co-located and P-to-S scattering does not occur for energy backscattered at angles of 180°, as we will show in a later section. The large separation in time between the P- and S-waves on the seismograms is caused by the strong contrast in sedimentary velocities by a factor of over 12. This was another reason to exclude S-waves from the 2-D FD calculations, because the computation of these long travel times would have taken too much CPU time for each model.

The 3-D migration of the waveforms was performed similar to the 2-D case with the addition of the 3rd dimension. In the following, the migration results will be presented as fence diagrams and slices though the 3-D model to reduce the data size and simplify their presentation. Two vertical slices through the migrated data cube are shown in Figure 40 in form of a fence diagram. The migration used the P-wave scattered data generated with 5 kHz source pulse. The amplitude scale is the same as in the 2-D case, with the maximum amplitude of the migration normalized to 1. The amplitude images of the located UXO are clearly visible in Figure 40, where the white circles indicate the actual locations of the spherical UXO. It can be seen that, similar to the 2-D case, the energy is mostly reflected off the top half of the UXO, such that the maximum amplitudes are either relocated directly on top, or along the upper side of the UXO facing the center of the array. The noise level throughout the background is relatively low with values up to 0.2, such that the UXO are easily located within the investigated block. To improve the view of the UXO structures, three horizontal slices at their respective depth are presented in Figure 41. Again, the white circles indicate the locations of the UXO. The image indicates how well the UXO are located in space and how confined their amplitude structures are. The noise level in the horizontal plane appears even lower than in the vertical planes. This example shows how a well-designed 2-D array can be used to locate

objects in 3-D space. It should be pointed out that number of sources and receivers is similar to the 2-D case in Tasks 3.

3-D Imaging of UXO with Noise-Contaminated Data

To investigate the sensitivity of the 3-D migration to noise, we added 50% Gaussian distributed uncorrelated noise to the seismic data. The result of this test is presented in Figure 42, where it is difficult to recognize the UXO reflections that were previously seen in Figure 39. The 3-D migration result of the noisy data is shown in Figure 43. The amplitude signatures of the UXO are clearly visible in the fence diagram, while the background noise is slightly elevated over the noise-free case with a level of approximately 0.25. The horizontal images, presented in Figure 44 show a similar result. The reason that the noise level appears elevated for the top-most slice lies in the fact that the amplitudes were re-normalized to 1, which also raised the noise level. The ratio of the UXO signature with respect to the background noise is actually the same in Figures 43 and 44. The two bottom slices show equally good results with a noise level of about 0.25. The example shows that the spatial density of receivers in the array does not have to be very high to overcome severe noise conditions.

3-D Imaging of UXO with 15 kHz Data and 1-D Source-Receiver Arrays

Once the UXO is detected and located in space it is worthwhile considering to increase the resolution by increasing the frequency of the seismic signal and utilizing a 1-D source-receiver array positioned above the UXO. For this investigation the 3-D analytical modeling is repeated using a 15 kHz source signal and the two UXO located in the xz-plane, while a source-receiver array with 31 elements each is located between x= 2 m and 4 m. The resulting waveforms are presented in Figure 45, where the P- and the S-wave are distinguishable by their different move-out and arrival time. Only two wave groups are visible for the P- and S-waves indicating the presence of two UXO in the subsurface. The higher frequency content of is apparent by the sharpness of the pulses. The migration result of the P-wave data is given in Figure 46. The location of the two UXO is the same as before. The aforementioned distribution of the amplitudes along the top of the UXO is particularly visible in this example. The amplitude structure for the top UXO is distributed around its top, mimicking its shape in the process. The reason for the shape of the image is the large aperture of the array, which illuminates the UXO over a large angular range. For the same reason, the 2nd, deeper located, UXO has a narrower amplitude structure along its top. The noise level in the background is relatively low with average values below 0.05.

3-D Imaging of UXO with 15 kHz S-Wave Data

It can be seen from the seismogram in Figure 45, that for most of the traces the S-wave amplitudes are larger than those of the P-waves. The reason lies in the physics

associated with the elastic scattering of acoustic waves. When a P-wave is incident upon an object, like a spherical shaped UXO, secondary P-waves as well as S-waves are scattered in all directions. In most cases P-to-S scattering produces larger amplitudes than P-to-P scattering (with the exception of very high frequencies, when the wavelengths are much smaller than the scattering object). The scattering process for a 15 kHz P-wave is presented in the scattering diagram in Figure 47. In the figure the scattered amplitudes are shown as a function of angle for a P-wave incident from below. The left and right half of the diagram show P-to-P and P-to-S scattering, respectively. It can be seen that for most backscattered angles (with the exception of 180°) the scattered S-wave is larger than the scattered P-wave. The fact that the scattering diagram has a notch for P-to-S backscattering at -180° explains why no S-waves were visible on the first trace of the seismograms in Figures 39 and 45. Because the P-to-S scattering is relatively strong, it is of interest to further investigate the S-wave data. The result of the S-wave migration is presented in Figure 48. It can be seen that the amplitude structure is rather distinct from that of the P-wave migration. The lines of the circles, denoting the locations of the UXO, are dotted, to avoid obscuring the amplitude structure of the migrated image. It is evident that the amplitude maximums appear on each side of the UXO rather than in the center on top, which is caused by the notch in S-wave amplitudes for straight backscattering. However, the amplitude structure complements that of the P-wave and adds independent information to the location process. Furthermore, the distinct scattering of P- and S-waves can help to characterize UXO once they are located and help to distinguish them from other objects. This is even more enticing as P-to-S scattering excites larger amplitudes than P-to-P scattering in most cases. The fact that S-waves are difficult to propagate in the seafloor sediments should not distract from the advantages that may become available if one succeeds in S-wave propagation. One option could be the excitation of S-waves with a wavelength similar to that of P-waves. These S-waves would have the same resolving power as P-waves but may propagate longer distances that those S-waves that have the same frequency as P-waves but much shorter wavelength. This topic warrants further investigation, because the advantages of the availability of both P- and S-waves for UXO discrimination are numerous.

Selective Focusing with D.O.R.T.

The decomposition of the time reverse operator or D.O.R.T. (Prada et al., 1996) is a method used in acoustics to direct energy onto specific targets under investigation. Similar to the array techniques described in the previous section, D.O.R.T. focuses energy onto selected scatterers by steering an array of sources using the eigenvectors and eigenvalues of the backscattered wavefield. The principle of the method is presented in Figure 49, where an array of l sources and m receivers is assumed in addition to two scatterers of different strengths located in the medium. Each source l is fired and the resulting wavefield recorded at each of the m receivers. The resulting waveforms are stored in the lth row of the matrix K_{lm}, and the successive firing of all sources will result in a full matrix K_{lm}, which contains the total scattered field of the inhomogeneities. The time reverse operator T_{lm} is subsequently constructed by

$$T_{lm} = K^{*}_{lm} K_{lm} ,$$

where K^{*}_{lm} denotes the conjugate-complex of K_{lm} . The singular value decomposition of T_{lm} yields

$$T_{lm} = V_{li} \ \Lambda_{ij} \ V^{H}_{jm} ,$$

where the eigenvectors are given by V_{li} and the eigenvalues by Λ_{ij}. Both properties are used to steer the array and focus energy onto selected targets in the medium. Figure 50 shows the eigenvalues as a function of frequency for the given example of the two scatterers in Figure 49. The eigenvalues are ordered by strength of scatterers such that eigenvalue #1 and #3 are related to the strong and weak scatterer, respectively (eigenvalue #2 is not developed in the current example and is associated with background noise). Eigenvalue #1 and its associated eigenvector can now be used to steer the array to focus onto the stronger of the two scatterers. This principle is presented in Figure 51, where the phase (or time delay) of each source is given by eigenvector #1 and the magnitude of each source is given by eigenvalue #1. The result of the focusing is shown in Figure 52, where snapshots of the FD simulations are shown, representing the propagating waves in the medium. Figure 52a depicts the situation shortly after the sources were fired and the wavefront starts to focus on the stronger scatterer. After more time has passed the waves have reached the inhomogeneity and the concentration of energy onto the stronger scatterer becomes evident in Figure 52b. The opposite case is presented in Figure 53, where the source array is steered to focus energy onto the weaker scatterer. The D.O.R.T. algorithm can thus be used to illuminate selected scattering targets in the medium, while simultaneously decreasing backscattered energy from other objects. The algorithm does not require information of the background medium and works auto-adaptive in real time in the field. Therefore, it can be used to focus on selected targets during the discrimination stage to improve the signal-to-noise ratio. It should be noted, however, that the D.O.R.T. algorithm does not locate objects in space, but rather amplifies the backscattered energy of selected targets, while suppressing the signal from other objects. The application of D.O.R.T. to improve UXO detection, localization, and discrimination seems enticing and should be further investigated.

Conclusions

Seismic arrays are very well suited for focusing energy onto specific targets under investigation particularly in relatively homogeneous media where the velocities of the propagating waves are known, such as in water. While the chances of detecting UXO are comparable between an array located in the water column and an array located on the seafloor, the latter has much better resolution, because of the proximity to the UXO. Additionally, the application of 3-component motion sensors in a seafloor array will increase the resolution of the location method - and eventually of the discrimination as well. Low signal-to-noise situations can be overcome by the use of source-receiver arrays, where the ability to stack can enhance seismic UXO signatures that otherwise remain undetected. There are currently worldwide efforts under way to develop

monitoring techniques based on stacking approaches that are capable of detecting minute signals from remote sources in noisy environments. The application of array techniques to UXO detection and localization follows the same principle.

The detection of proud objects is feasible as long as the contrast in elastic properties between the UXO and the surrounding medium is stronger than that across the seafloor interface. Larger array apertures can help to reduce the interference of the seafloor reflection.

It is promising that the dimensions of two UXO, separated by one third of the wavelength of the incident wave, can be resolved if the targets are located within a few wavelengths of the array.

The findings that the parameters of a rippled seafloor can be determined while UXO are correctly located in the sediments, even if a flat seafloor interface is assumed during the migration process, has far reaching consequences. The newly found interface parameters help to improve the velocity model, which increases the resolution of the applied method, and eventually will lead to better discrimination techniques that rely on seismic scattering. The fact that stacked amplitudes become strongest during the migration process when the correct velocity model is used allows this important parameter to be estimated during the location step. Furthermore, the result that a range of comparable velocity models yields similar location accuracy is also attributable to the use of a source-receiver array, which reduces small mislocation errors through stacking.

Careful analysis of 2-D arrays is needed prior to data acquisition to optimize its sensitivity with respect to the area under investigation. Once the array geometry is optimized, even sparse receiver arrangements can be utilized to locate UXO in space under adverse noise conditions. Although it is difficult to propagate S-waves in seafloor sediments, the advantages of using complementary S-wave information particularly for UXO characterization warrants investigations into how the waves can be excited and propagated. Studies with broadband signals need to be conducted to investigate if and at what frequencies S-waves can be propagated in the littoral environments. Because the S-wave velocity is rather low in seafloor sediments, even low frequency waves may have short enough wavelengths to provide sufficient resolution for UXO characterization. Yet these low frequency waves may be capable of propagating in the seafloor sediments.

The availability of auto-adaptive focusing methods like D.O.R.T., which was specifically developed for acoustic media, creates a good opportunity to study their applicability to UXO detection problems. If auto-adaptive focusing is feasible in field situations, the signal-to-noise-ratio of energy backscattered from selected objects can be improved over signals caused by background heterogeneity.

The characterization of UXO poses a challenge that needs to be thoroughly investigated. Once located in space, it is important to determine the type and possible the material properties of UXO. Scattering approaches appear to be the best method to solve this problem even if P-waves data were available only. Recent developments of innovative techniques to determine the elastic properties of medium inhomogeneities using scattered waves (Gritto, 1995; Gritto et al., 1999) offer the right tools to solve the characterization problem.

Literature

Gritto, R. (1995): Rayleigh scattering and nonlinear inversion of elastic waves, Ph.D. Thesis, University of California at Berkeley, pp. 129.

Gritto, R.; Korneev, V. A.; Johnson, L. R. (1999): Nonlinear Three-Dimensional Inversion of Low-Frequency Scattered Elastic Waves, *Pure and Applied Geophysics*, Vol. 56, LBNL-39281, pp. 557-589.

Hamilton, E. L., 1971, Prediction of in-situ acoustic and elastic properties of marine sediments, *Geophysics*, Vol. 36, No.2, p. 266-284.

Hamilton, E. L., 1972, Compressional-wave attenuation in marine sediments, *Geophysics*, Vol. 37, No.4, p. 620-646.

Hamilton, E. L., 1976, Shear-wave velocity versus depth in marine sediments: A review, *Geophysics*, Vol. 41, No.2, p. 985-996.

Kibblewhite, A. C., 1989, Attenuation of sound in marine sediments: A review with emphasis on new low-frequency data, *J. Acoust. Soc. Am.*, Vol. 86, No.2, p. 716-738.

Korneev, V. A. and Johnson, L. R., 1993a, Scattering of elastic waves by a spherical inclusion - 1. Theory and numerical results, Geophys. J. Int., Vol. 115, p. 230-250.

Korneev, V. A. and Johnson, L. R., 1993b, Scattering of elastic waves by a spherical inclusion - 2. Limitation of asymptotic solutions, Geophys. J. Int., Vol. 115, p. 251-263.

Lopes J. L., Nesbitt C. L., Lim R., Williams K. L., Thorsos E. I. and, Tang D., 2003, Subcritical Detection of Targets Buried Under a Rippled Interface: Calibrated Levels and Effects of Large Roughness, Proceedings Oceans 2003 Marine Technology and Ocean Science Conference, San Diego, CA.

Podvin, P. and Lecompte, I., 1991, Finite difference computations of travel times in very contrasted velocity models: A massively parallel approach and its associated tools, *Geophys. J. Int.*, Vol. 105, p. 271-284.

Prada, C., Maneville, S., Spoliansky, D., and Fink, M., 1996, Decomposition of the time reversal operator: detection and selective focusing on two scatterers, *J. Acoust. Soc. Am.*, Vol. 99, p. 2067-2076.

Stoll, R. D., 1985, Marine Sediment Acoustics, *J. Acoust. Soc. Am.*, Vol. 77, p. 1789-1799.

Figures

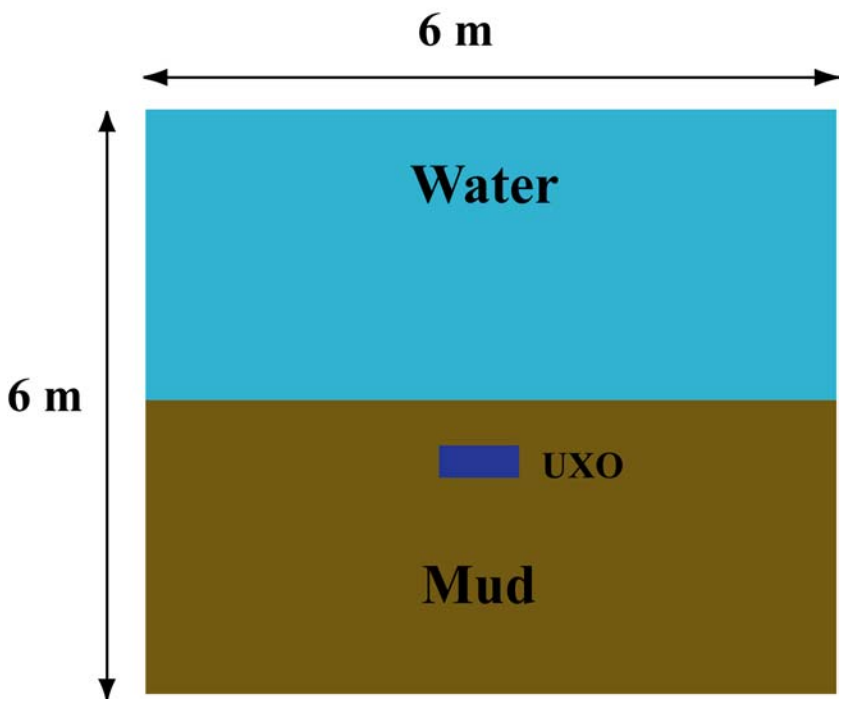

Figure 1: Schematic of the finite difference model

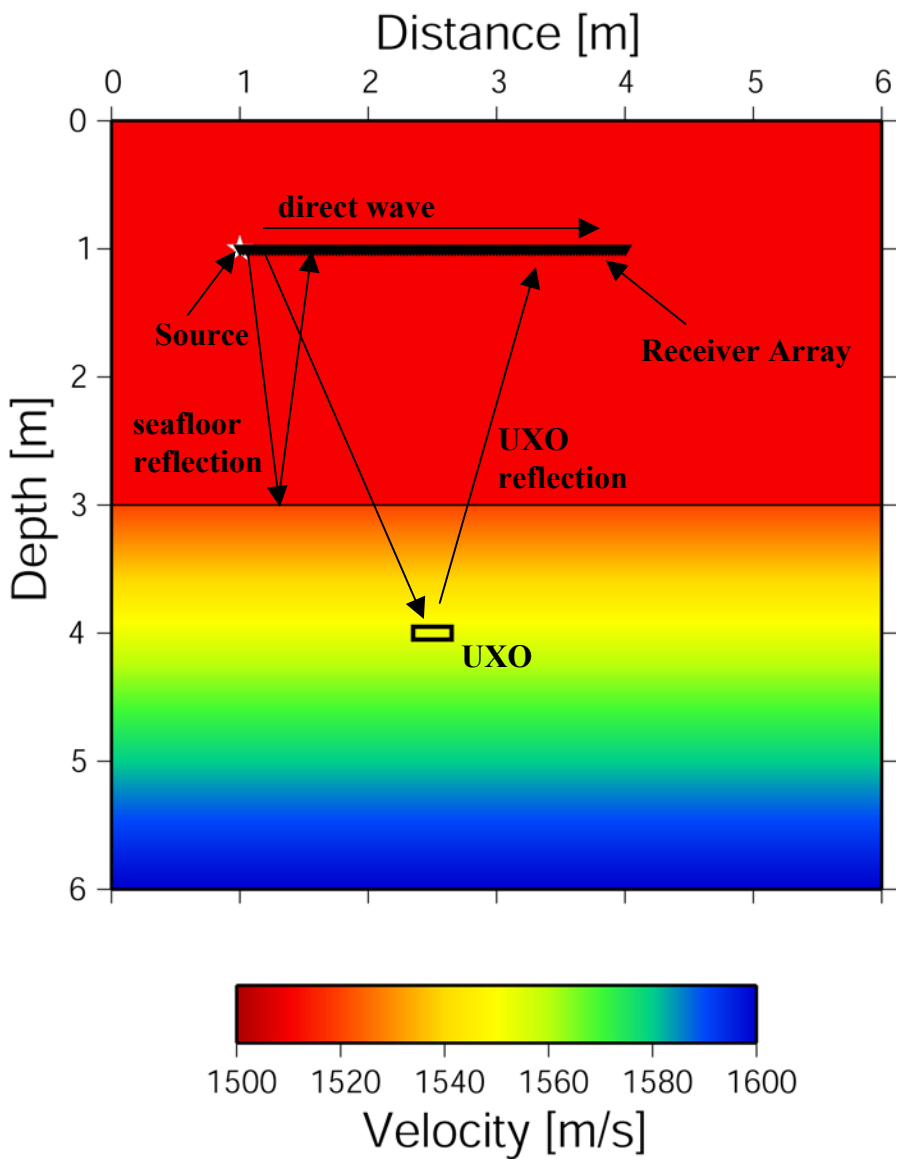

Figure 2: Velocity model derived from the parameters listed in Table 1. Source number one is indicated by the white star, while the receiver array, consisting of 31 sensors, is denoted by black triangles. The water layer is represented by the top 3 m, while the sediments are represented by the bottom half. The propagation paths of the three main wave groups are indicated by the arrows.

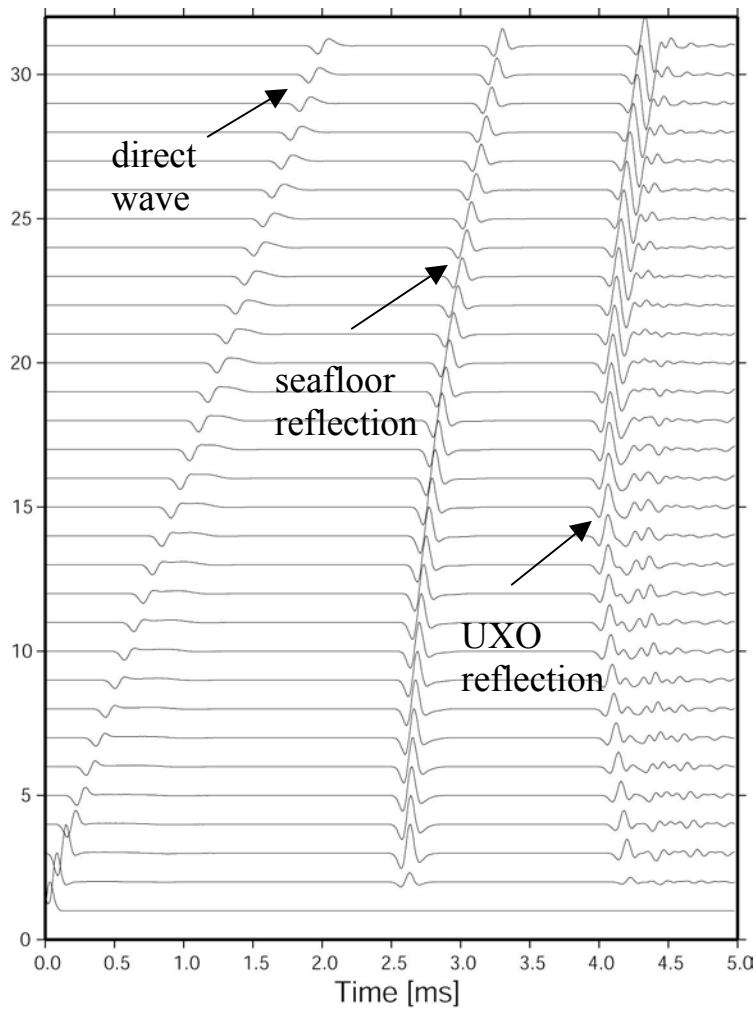

Figure 3: Seismic waveforms generated for the model shown in Figure 2. The source location was at x = 1 m and z = 1 m.

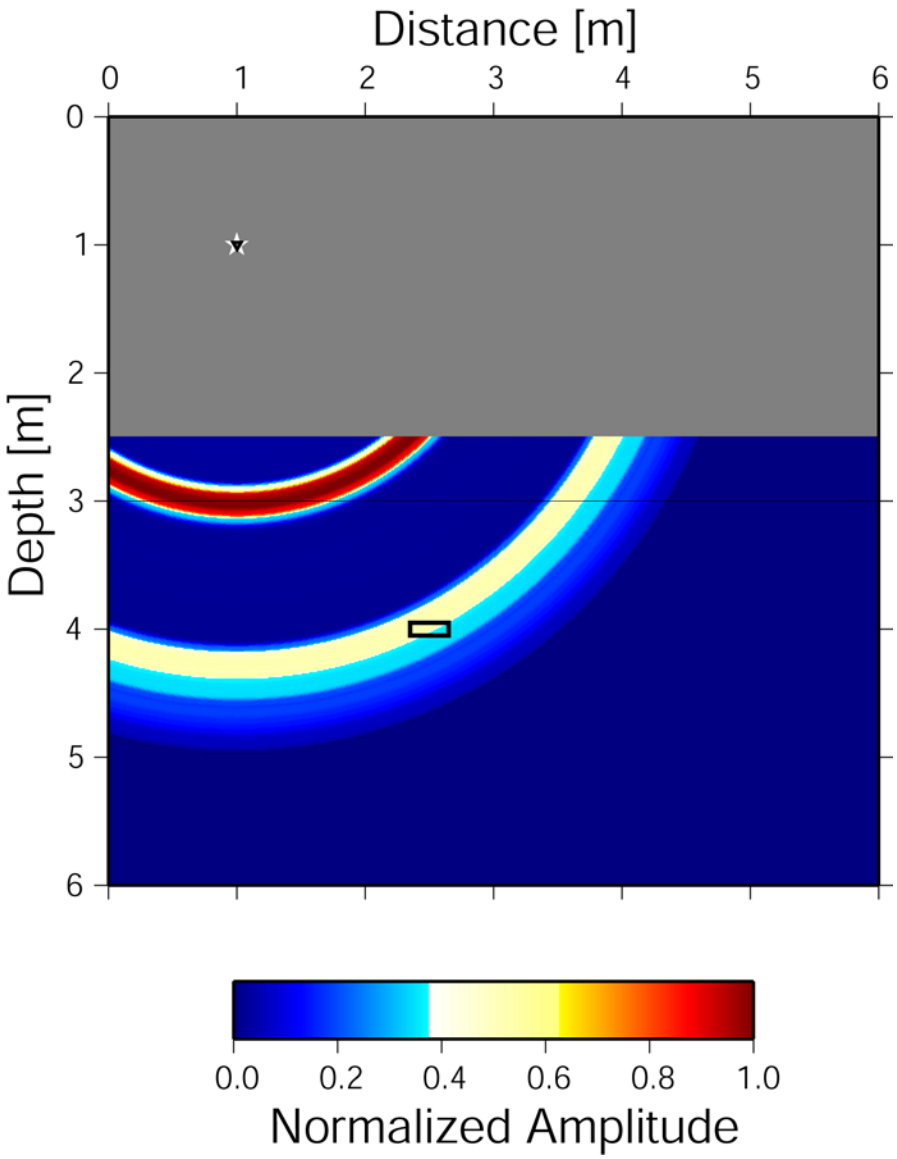

Figure 4: Migration result of a single source-receiver combination. The image is based on a source and receiver both located at x = 1 m and z = 1 m, indicated by the star and triangle, respectively. The migration was performed over a depth range from 2.5 m to 6.0 m excluding the gray area above the amplitude image.

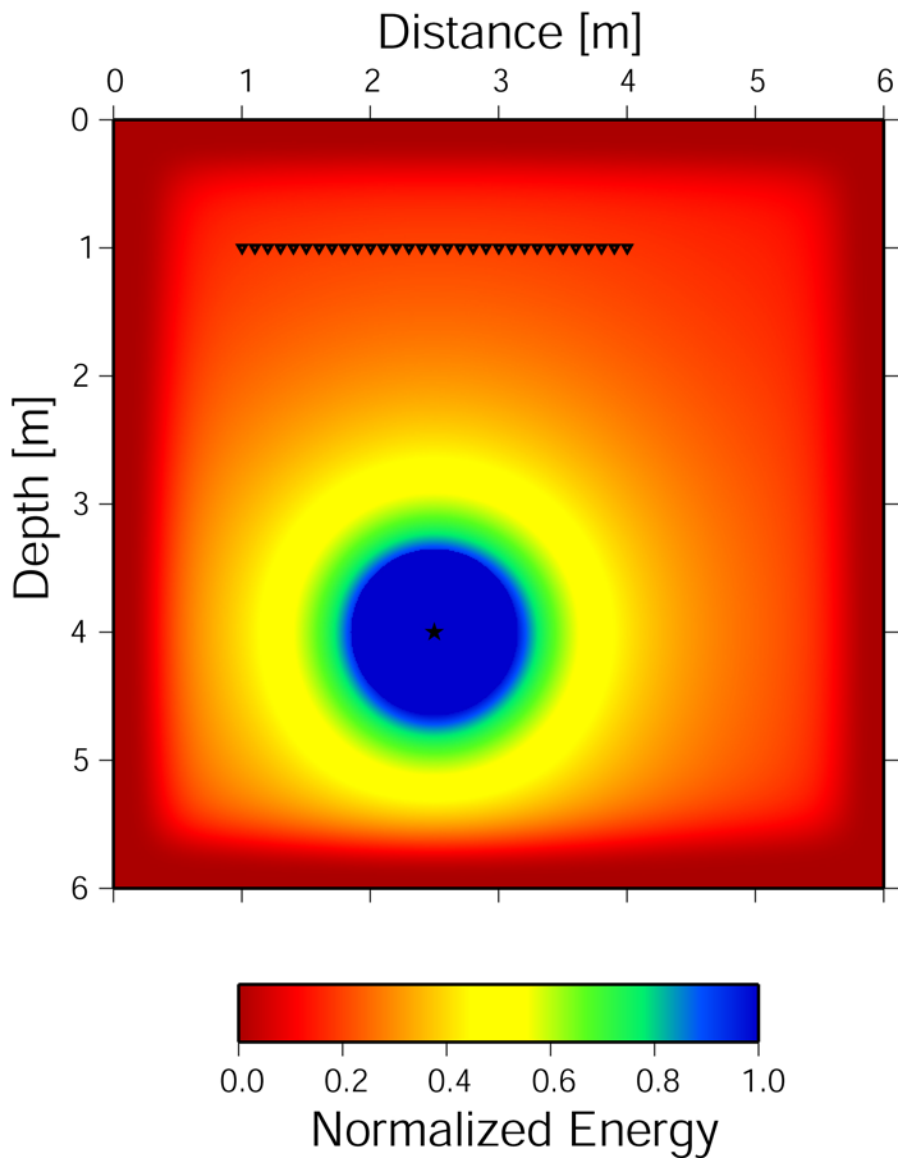

Figure 5: Energy radiation of a point pressure source located in a homogeneous medium. The gradual decay in radial direction is evident, while the energy in the central source region was normalized for plotting purposes.

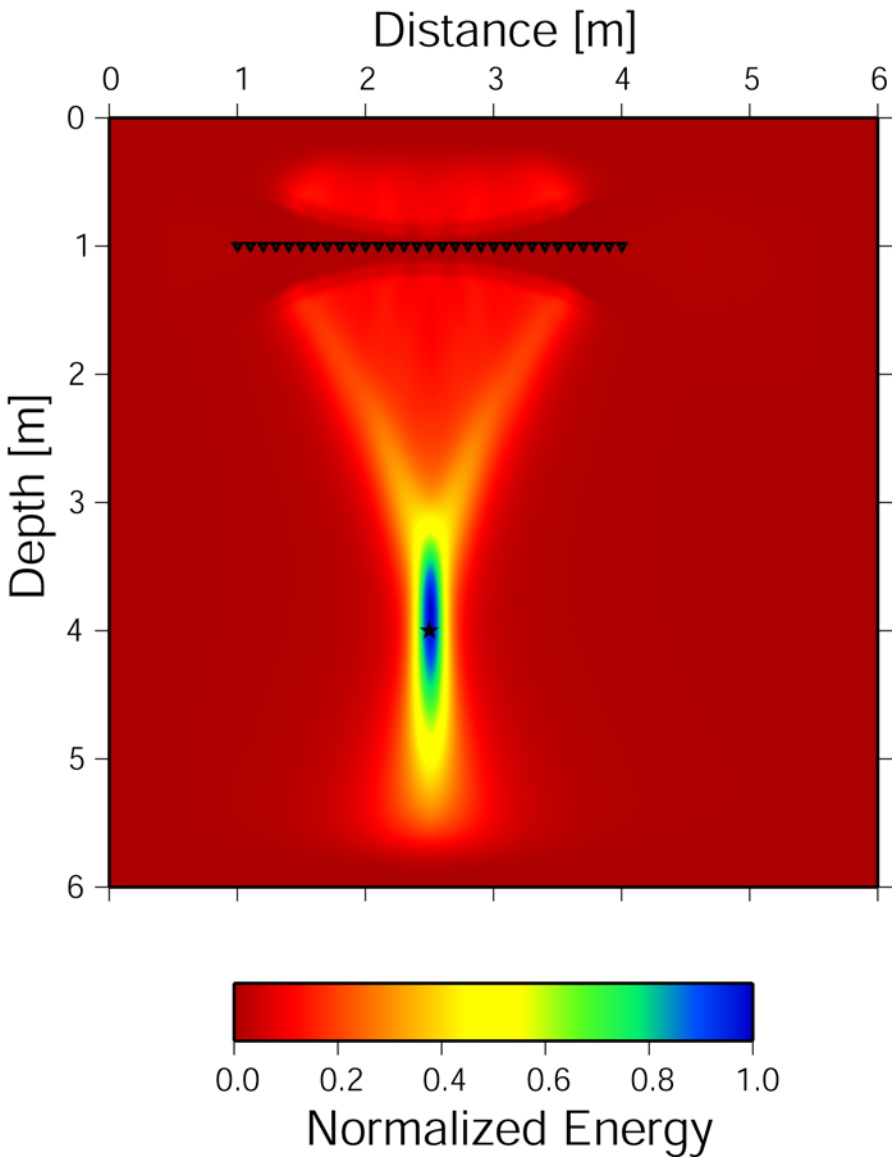

Figure 6: Result of focusing the receiver array to illuminate the source location. The recorded energy was emitted by the source in Figure 5.

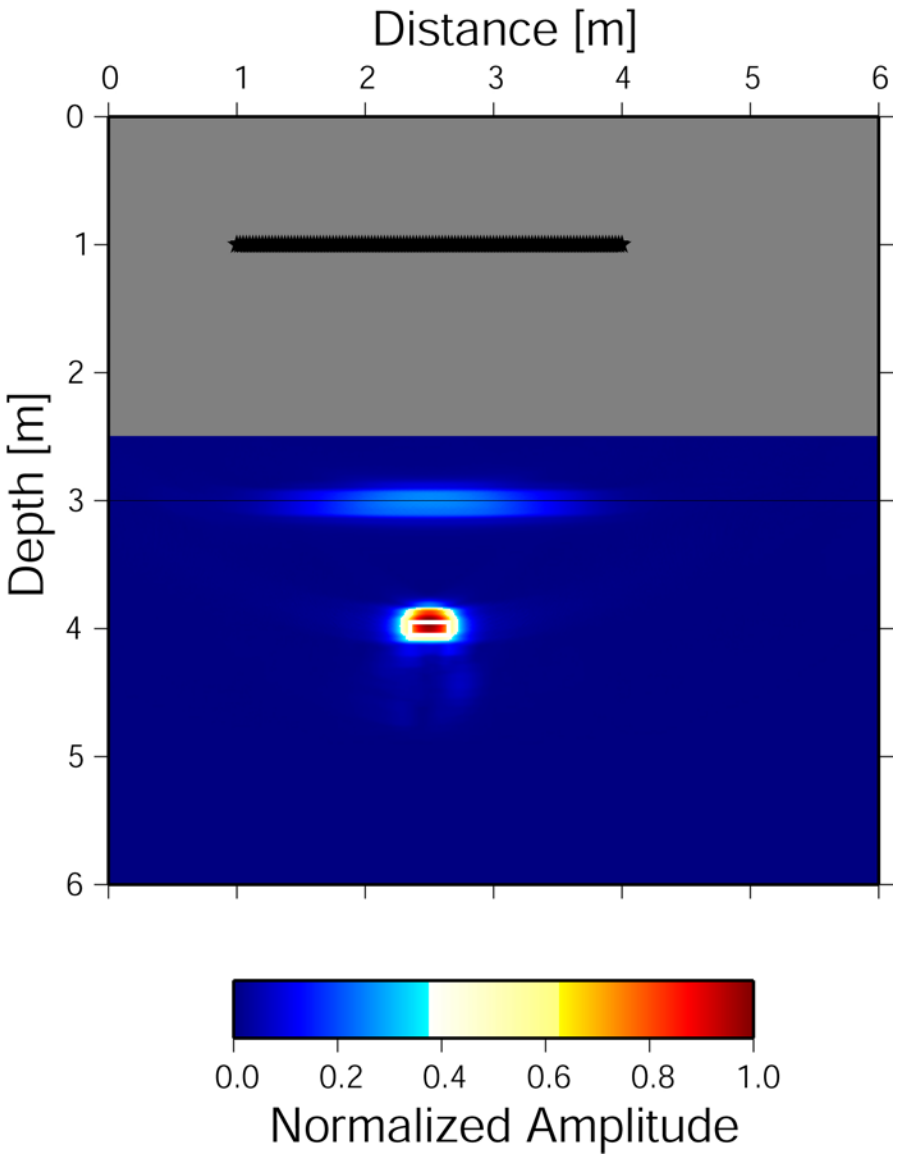

Figure 7: Normalized amplitude map of migrated waveforms recorded by 31 sources and 31 receivers in the source-receiver array, co-located at a depth of 1 m between x=1 m and x=4 m. The migration was performed over a depth range from 2.5 m to 6.0 m excluding the gray area above the amplitude image.

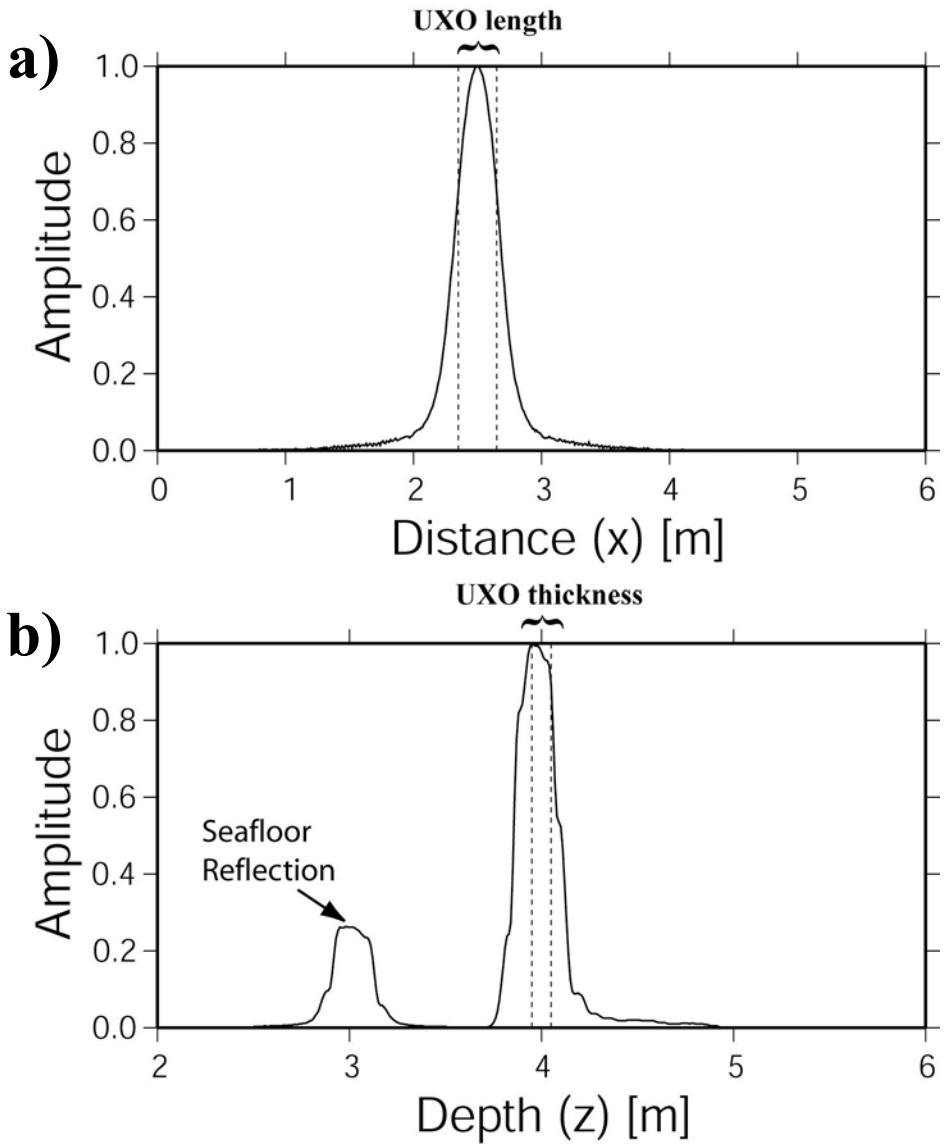

Figure 8: Cross sections of normalized amplitudes through the UXO signature in Figure 7. **a)** Cross section in x-direction.
b) Cross section in z-direction. The dashed lines in **a)** and **b)** indicate the width and thickness of the UXO, respectively.

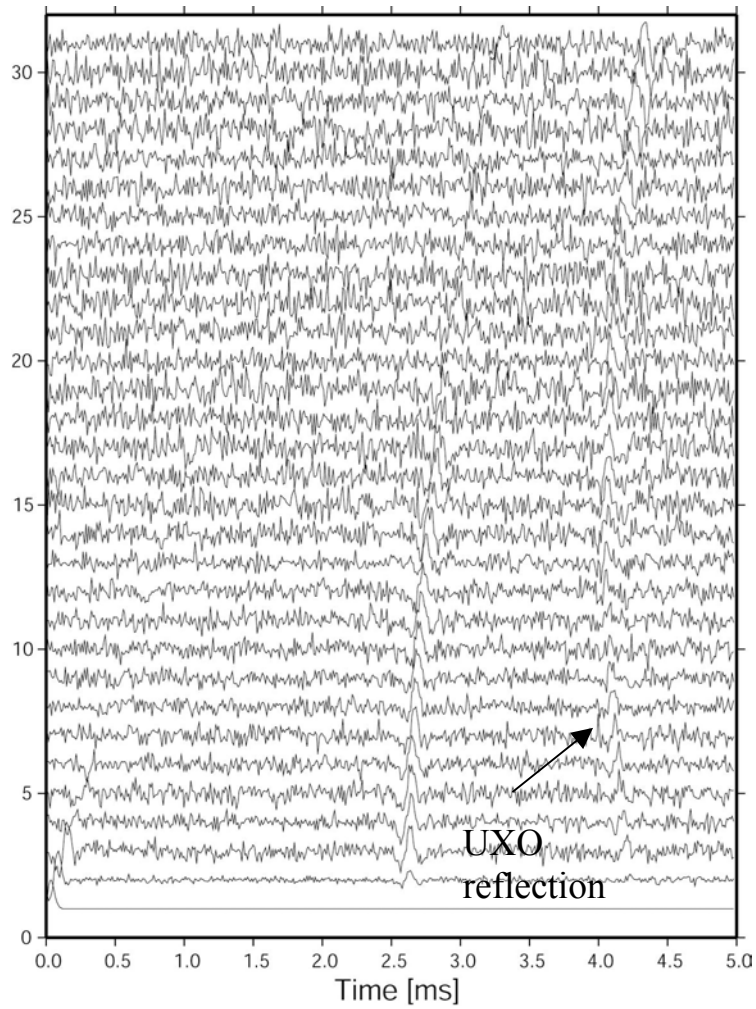

Figure 9: Same as Figure 2, with the addition of 50% Gaussian distributed noise.

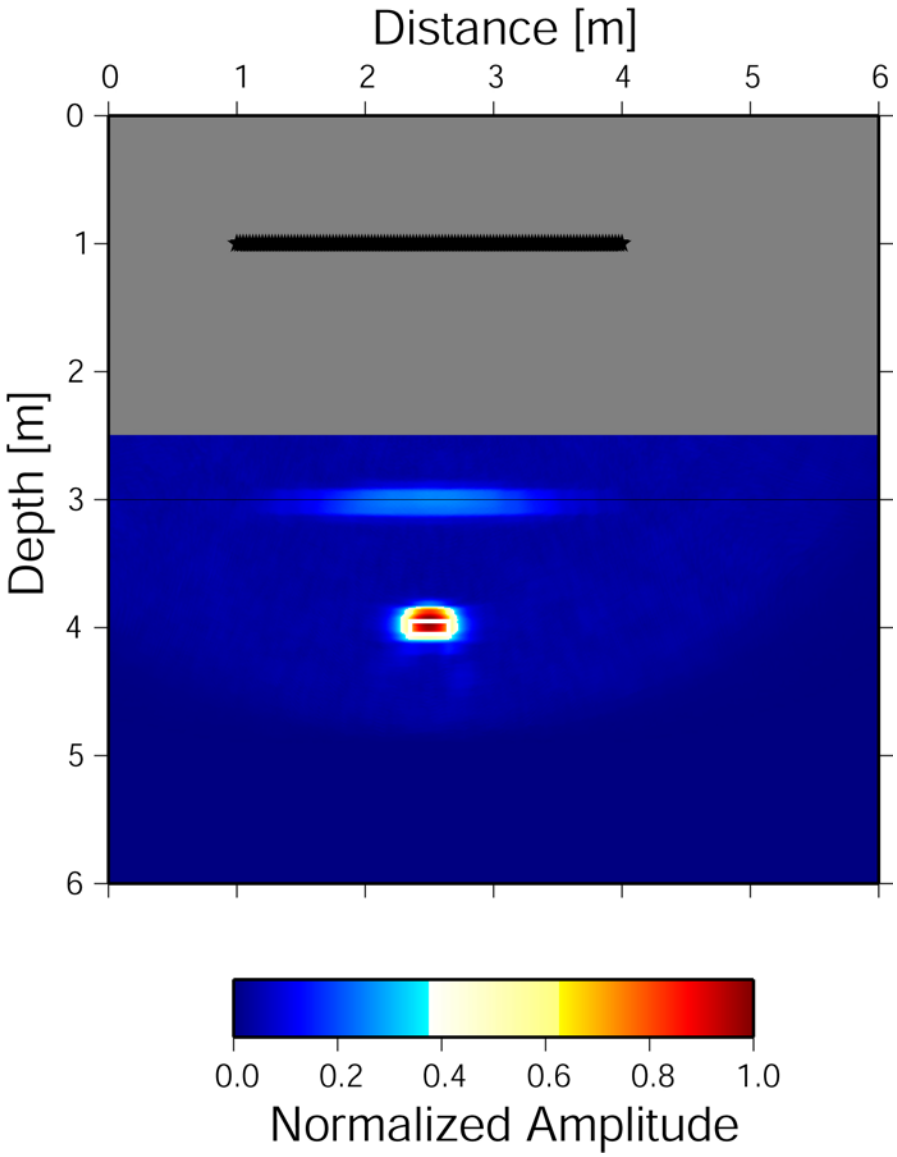

Figure 10: Normalized amplitude map of migrated waveforms recorded by 31 sources and 31 receivers in the source-receiver array. A noise level of 50% was added to the waveforms prior to migration. The migration was performed over a depth interval between 2.5 m and 6.0 m.

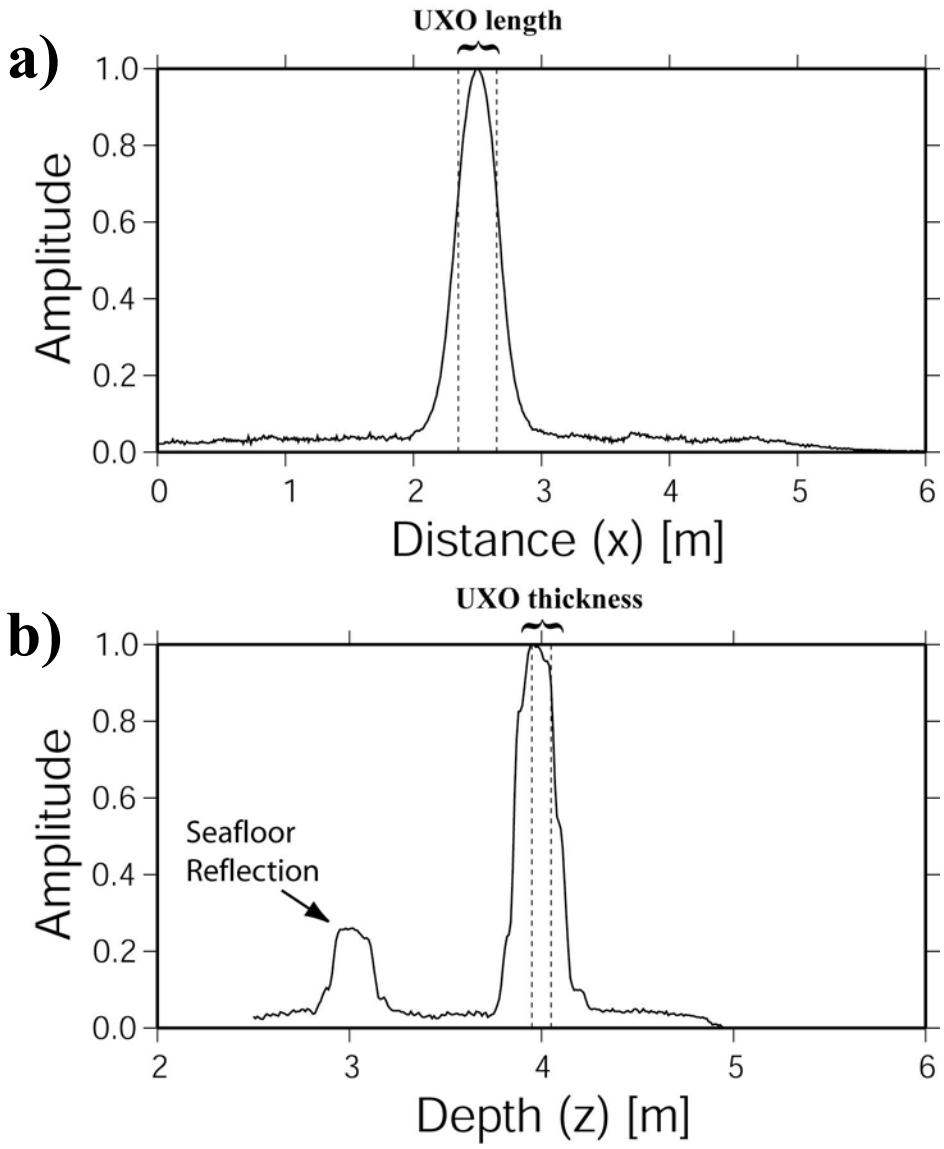

Figure 11: Cross sections of normalized amplitudes through the UXO signature in Figure 10. **a)** Cross section in x-direction. **b)** Cross section in z-direction.

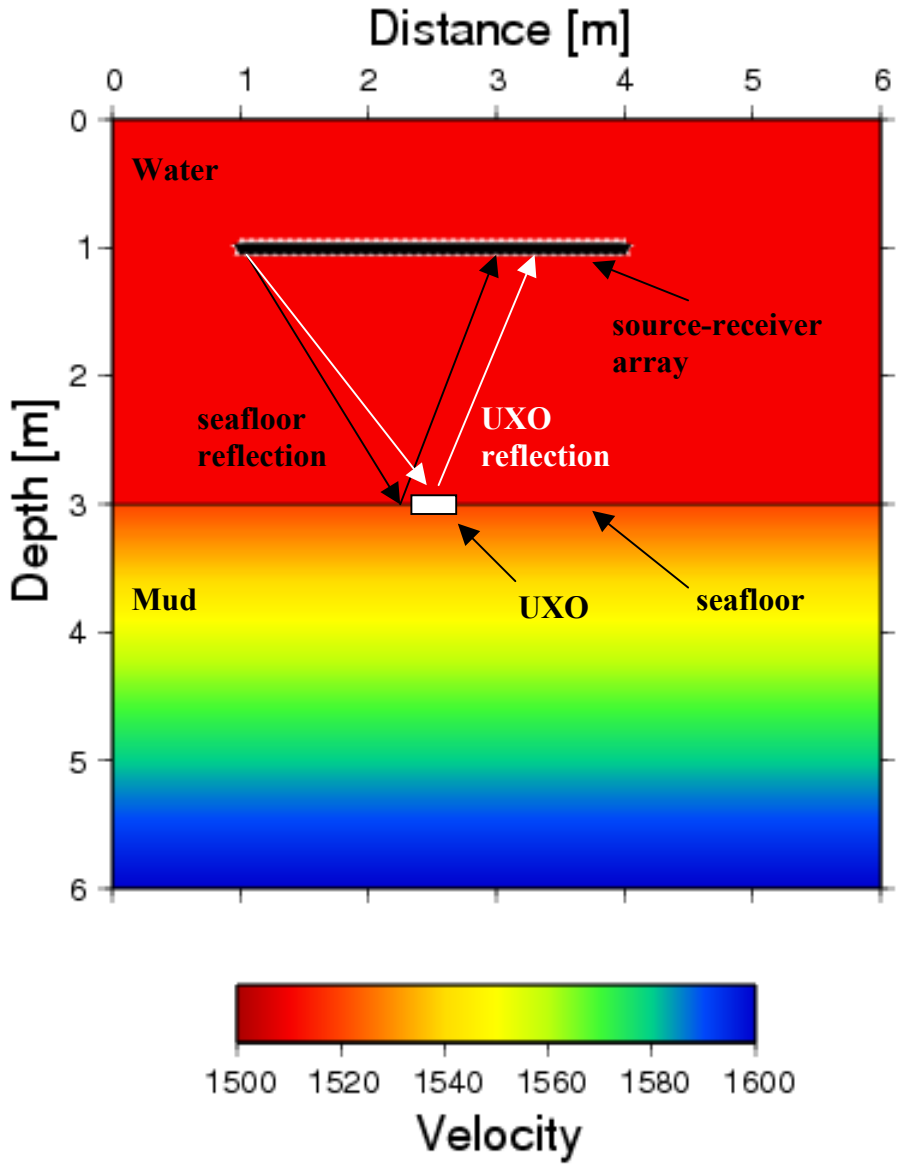

Figure 12: Velocity model and source-receiver array location for the case of a proud object (UXO half-buried in seafloor sediments). The proximity of reflection points on the seafloor interface and on the UXO produces reflections that are not separated in time no the seismograms (see Figure 13).

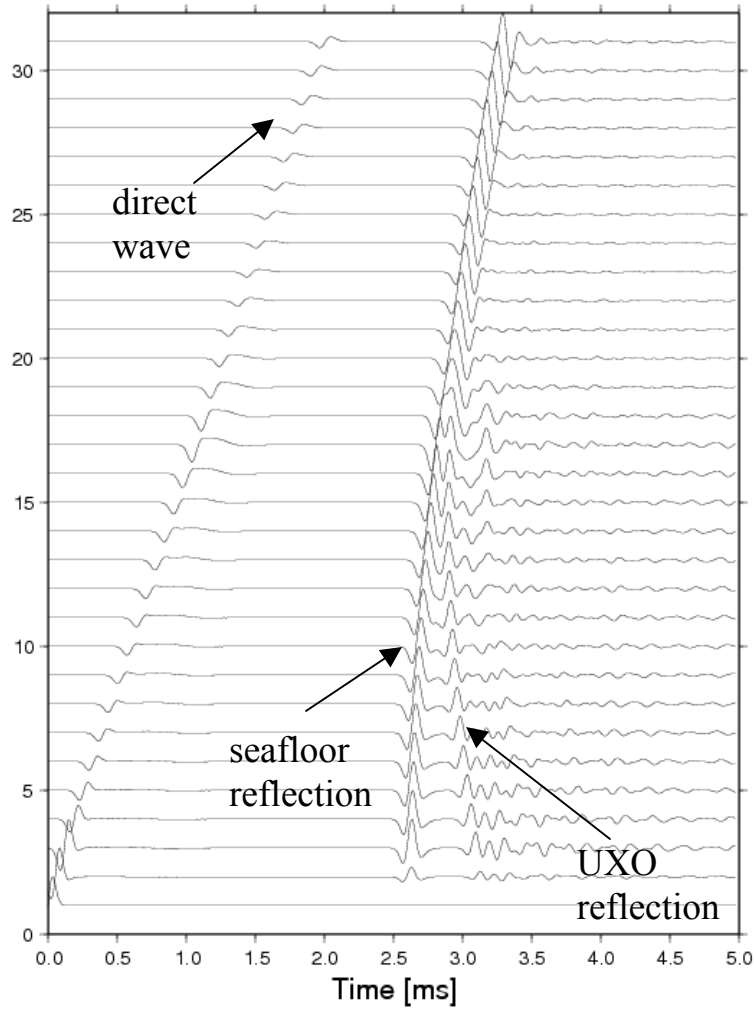

Figure 13: Seismic waveforms generated by the shot at x = 1m and z = 1 m and recorded by the receiver array, calculated for the model in Figure 12. For this source position, the seafloor and UXO reflections can be distinguished for the receiver locations close to the source (short offsets), but these arrivals merge to a single pulse for larger offsets.

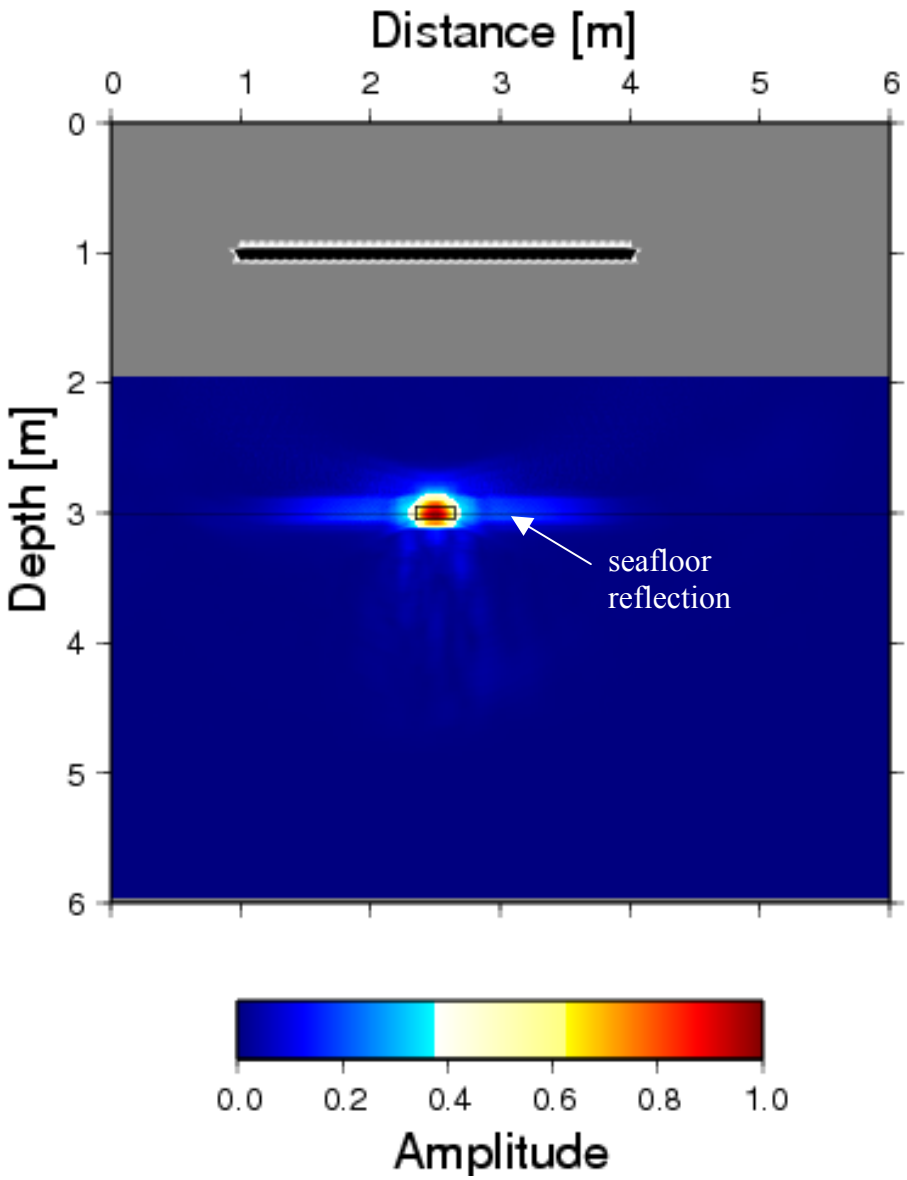

Figure 14: Normalized amplitude map of migrated waveforms recorded by the 31 sources and 31 receivers in the array for a UXO half-buried in the seafloor sediments (proud object). The migration was carried out over a depth interval between 2.0 m and 6.0 m.

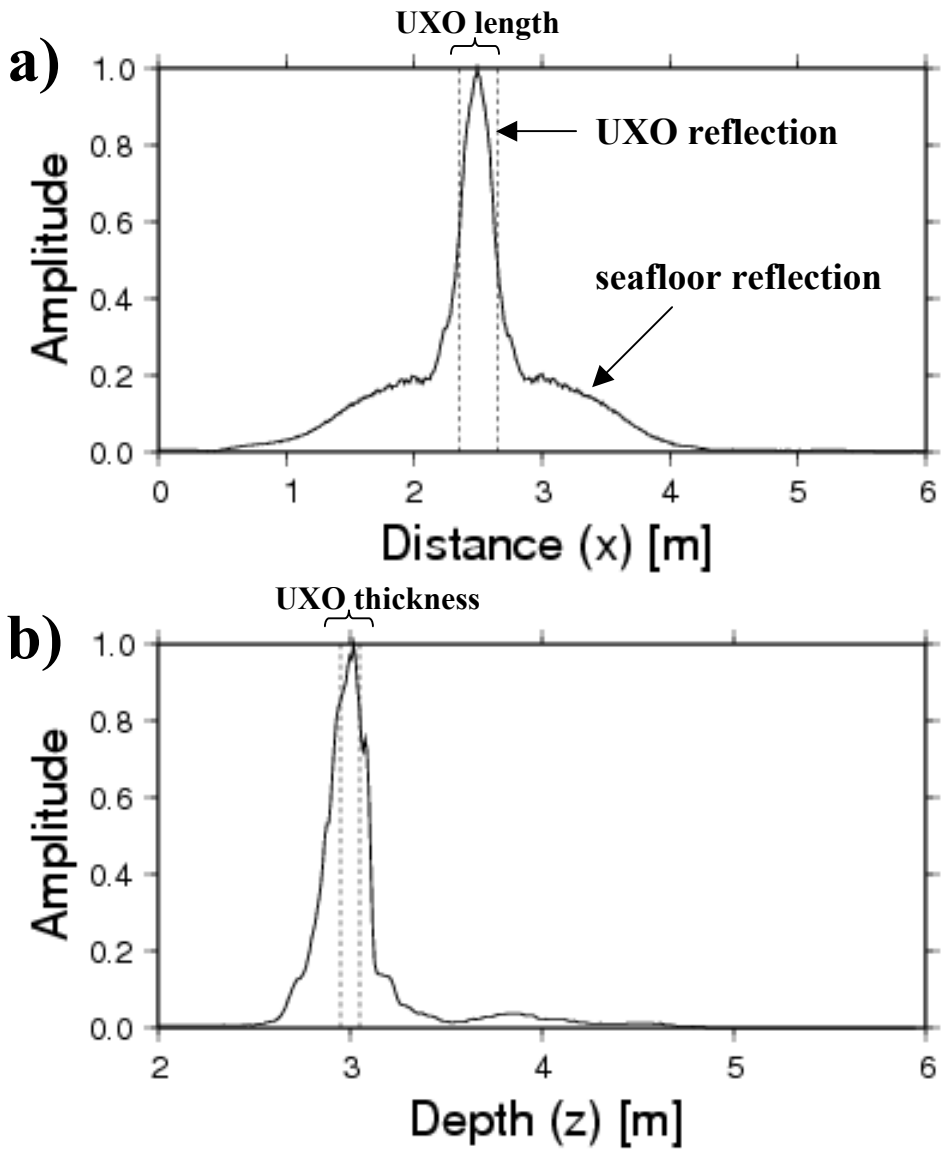

Figure 15: Cross sections of normalized amplitudes through the UXO signature in Figure 14. The seafloor reflection is represented by the elevated background amplitude in x-direction. **a)** Cross section in x-direction. **b)** Cross section in z-direction.

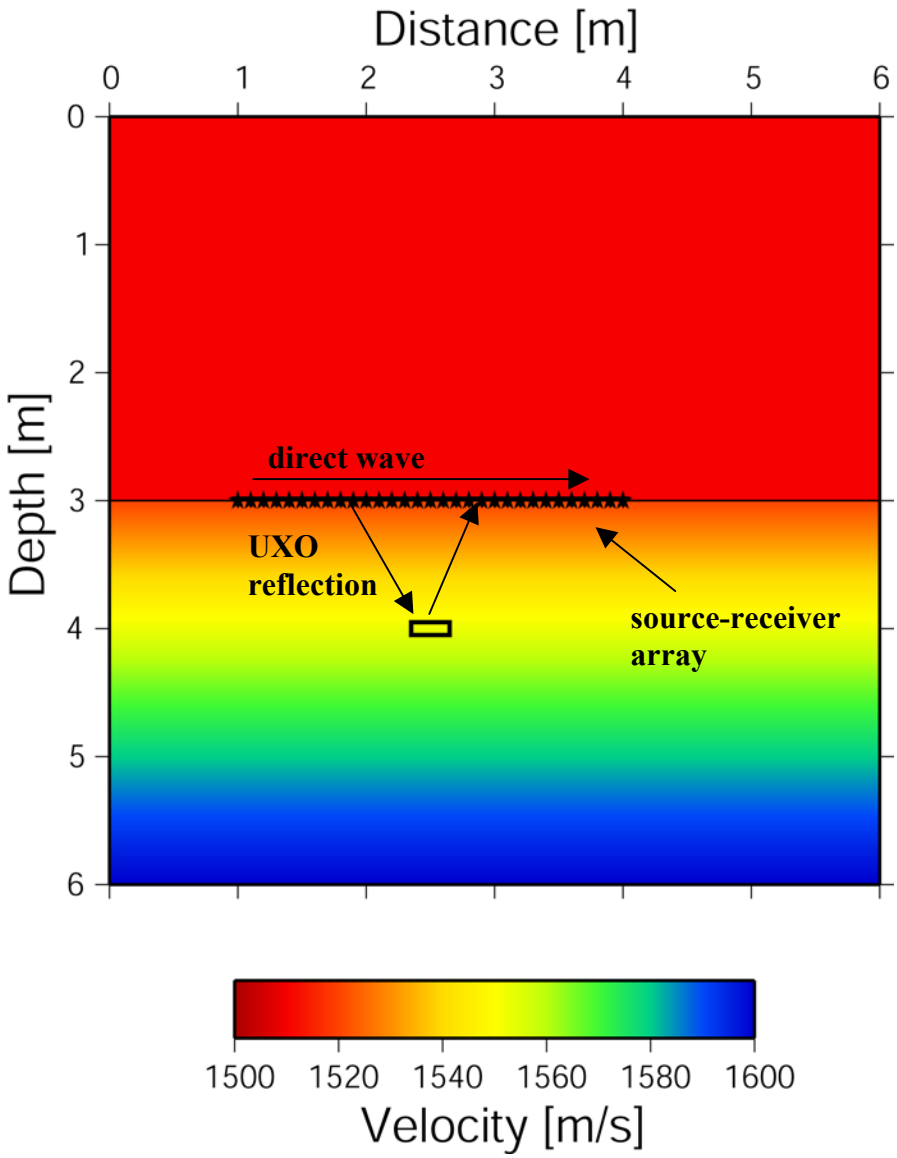

Figure 16: Same velocity model as in Figure 2, with source-receiver array consisting of 31 sources and 31 receivers, positioned along seafloor.

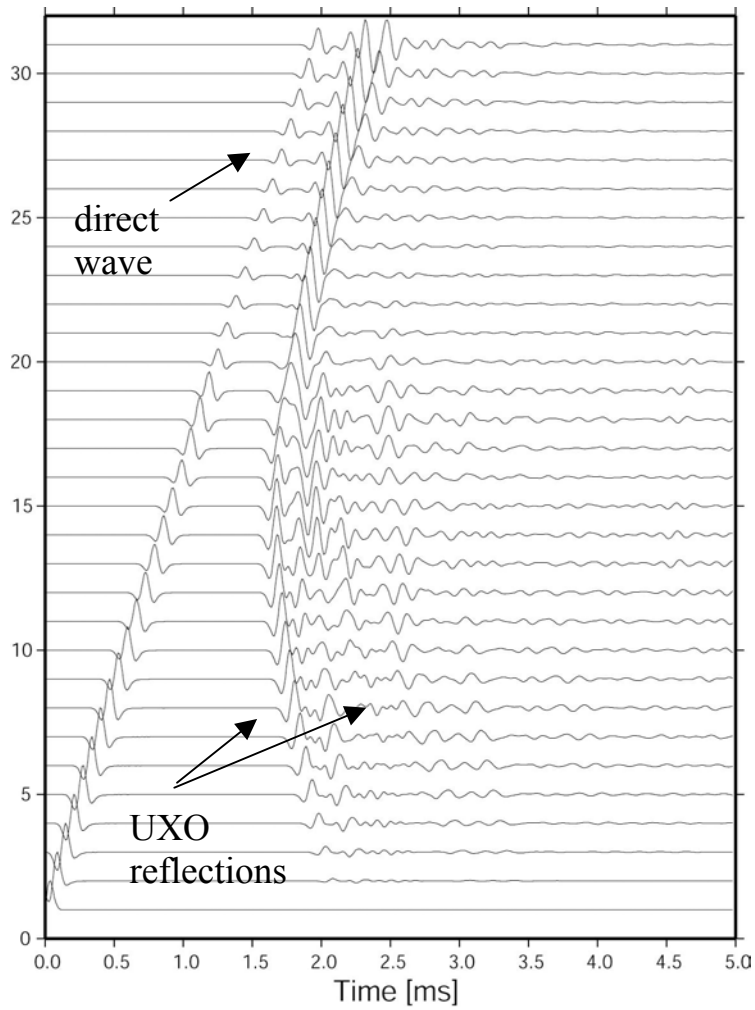

Figure 17: Seismic waveforms generated by the shot at x = 1m and z = 3 m and recorded by the receiver array with the model shown in Figure 16.

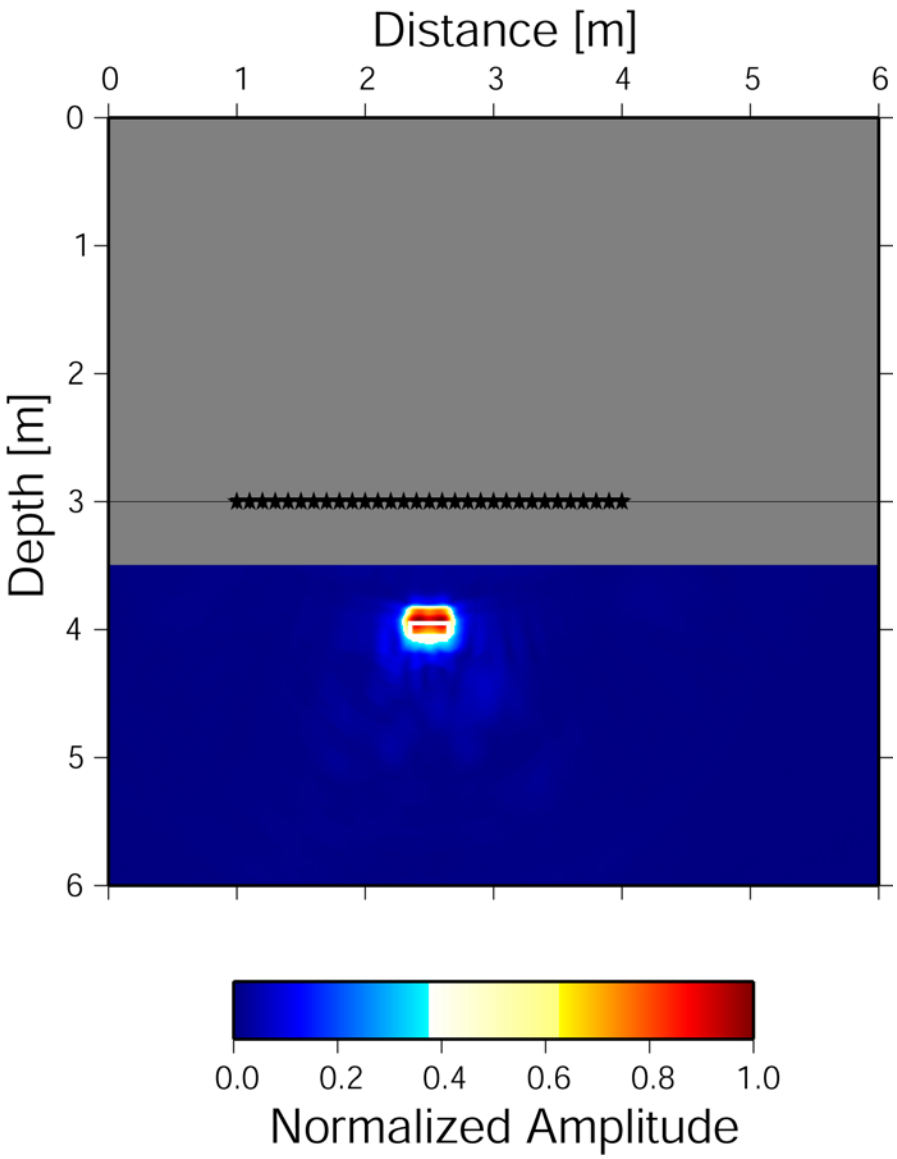

Figure 18: Normalized amplitude map of migrated waveforms recorded by the 31 sources and 31 receivers in the seafloor array. The migration was performed over a depth interval between 3.5 m and 6.0 m excluding the gray area above the amplitude image.

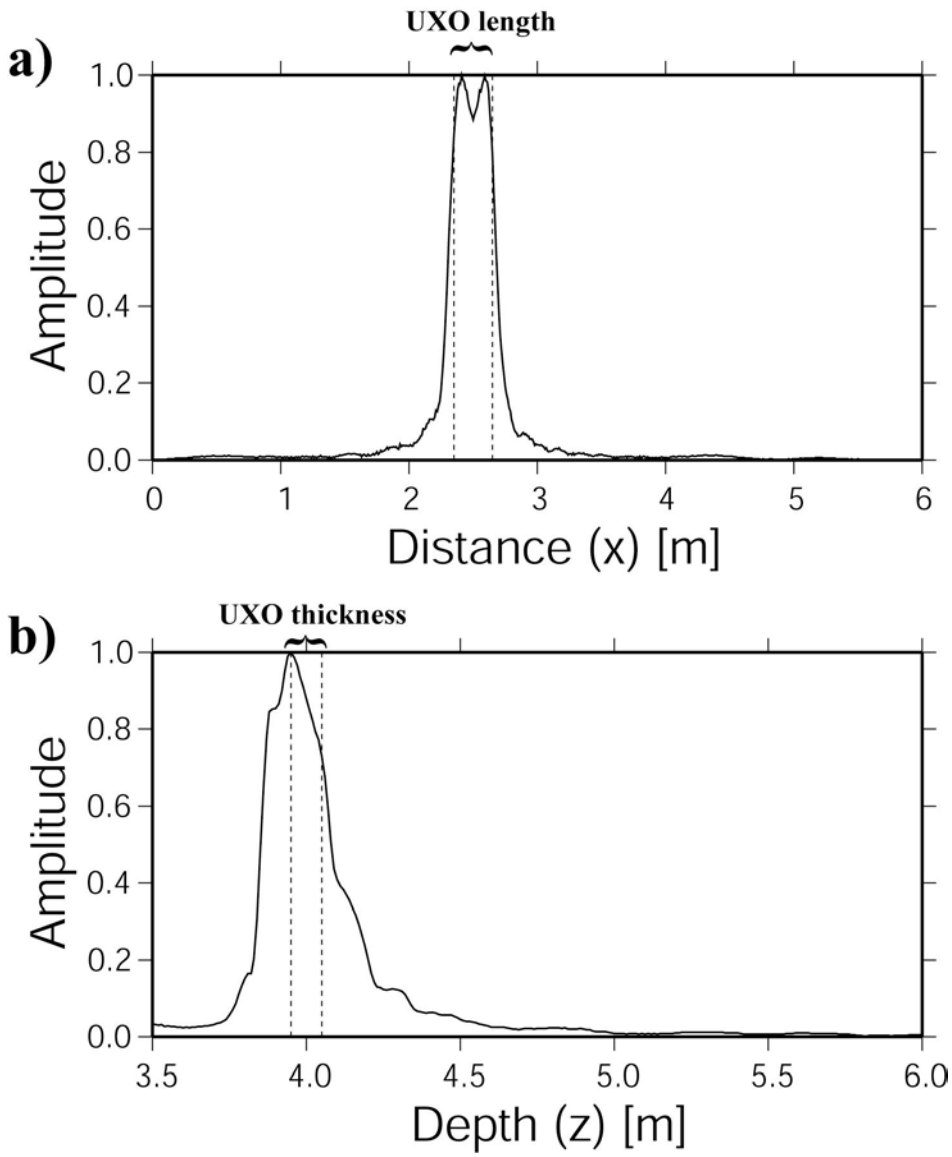

Figure 19: Cross sections of normalized amplitudes through the UXO signature in Figure 18. **a)** Cross section in x-direction. **b)** Cross section in z-direction.

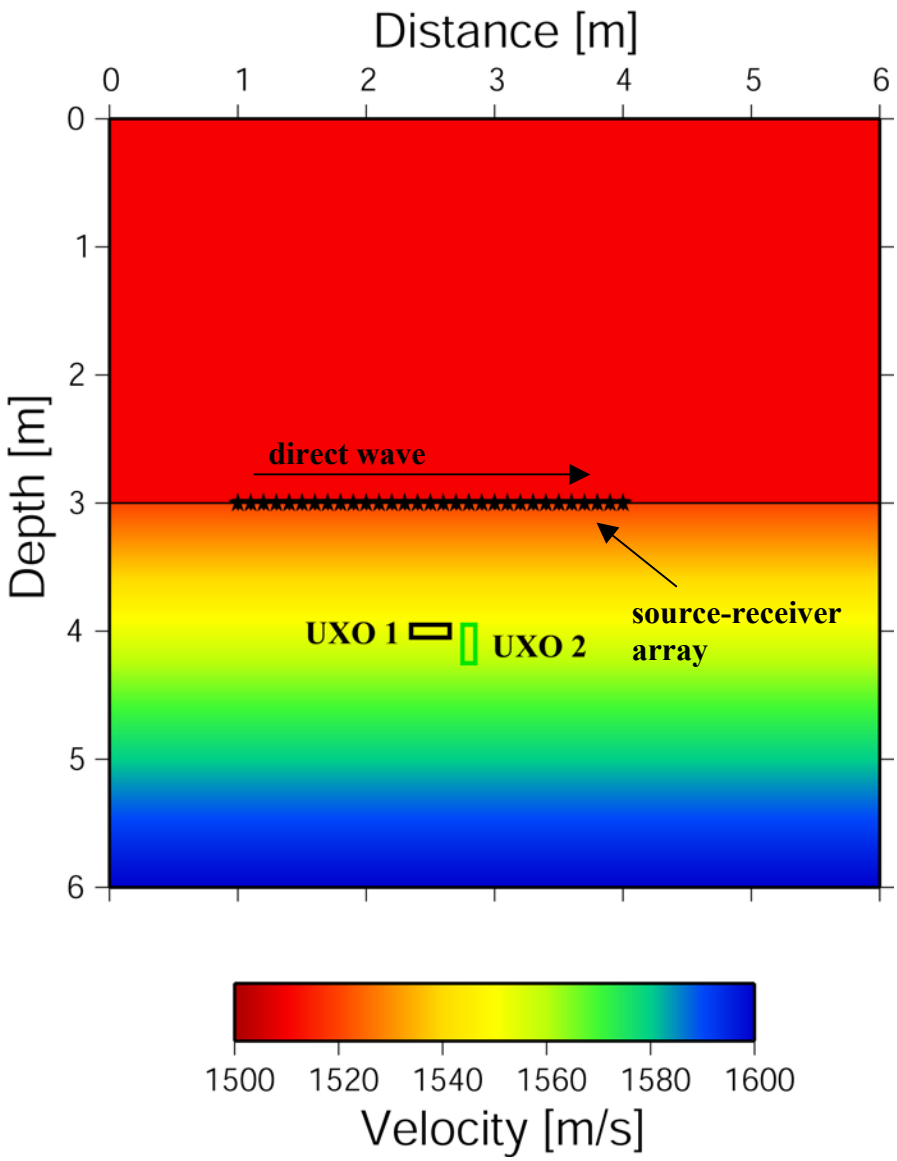

Figure 20: Same velocity model as in Figure 2, with source-receiver array positioned along seafloor. Two UXO are modeled and color-coded for better comparison with Figures 22 and 23.

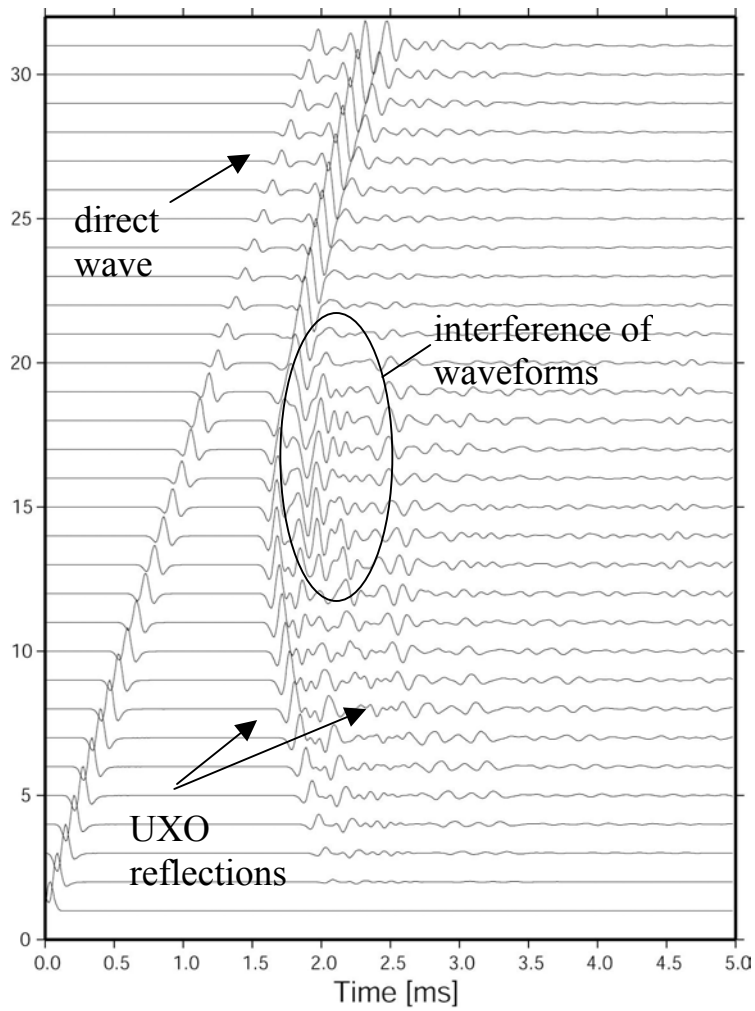

Figure 21: Seismic waveforms generated by the shot at x = 1m and z = 3 m and recorded by the receiver array with the model shown in Figure 20.

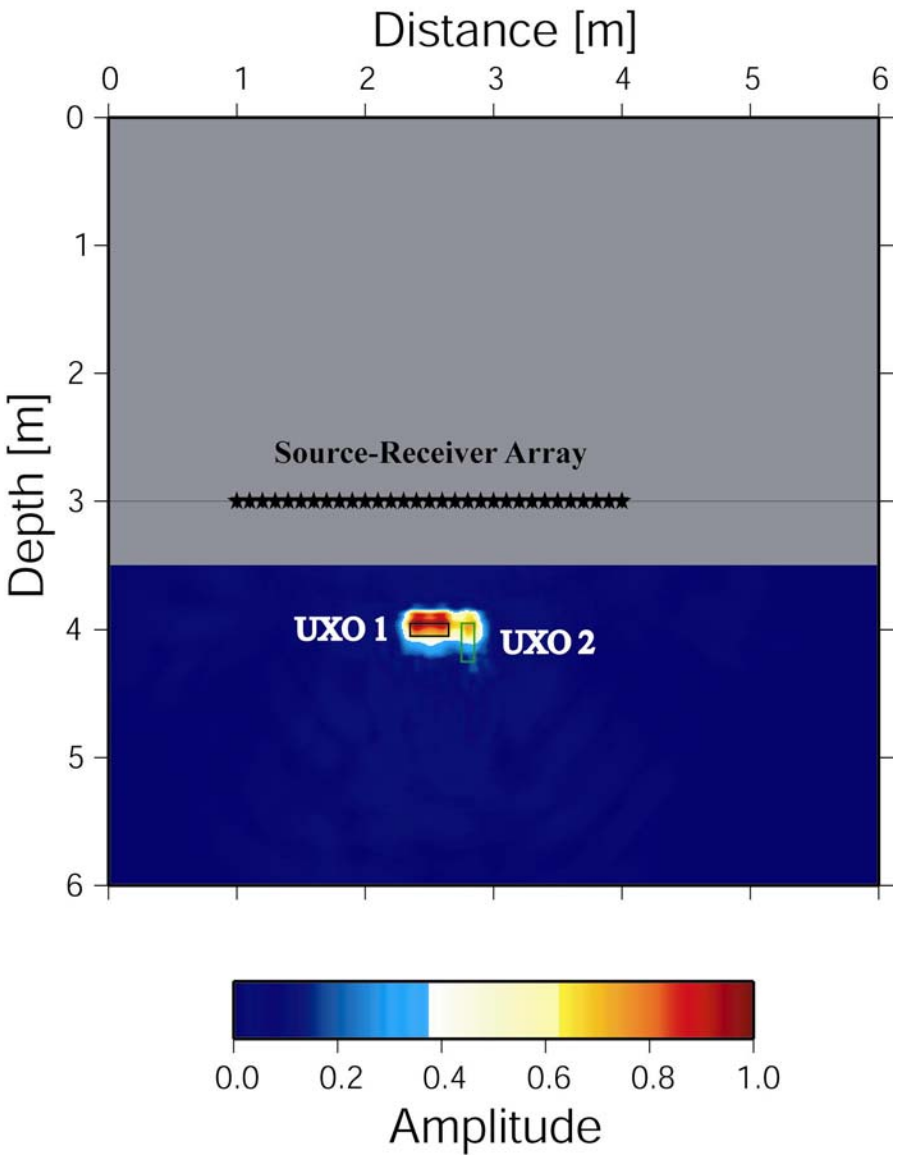

Figure 22: Normalized amplitude map of migrated waveforms recorded by the 31 sources and 31 receivers in the seafloor array. The migration was performed over a depth interval between 3.5 m and 6.0 m.

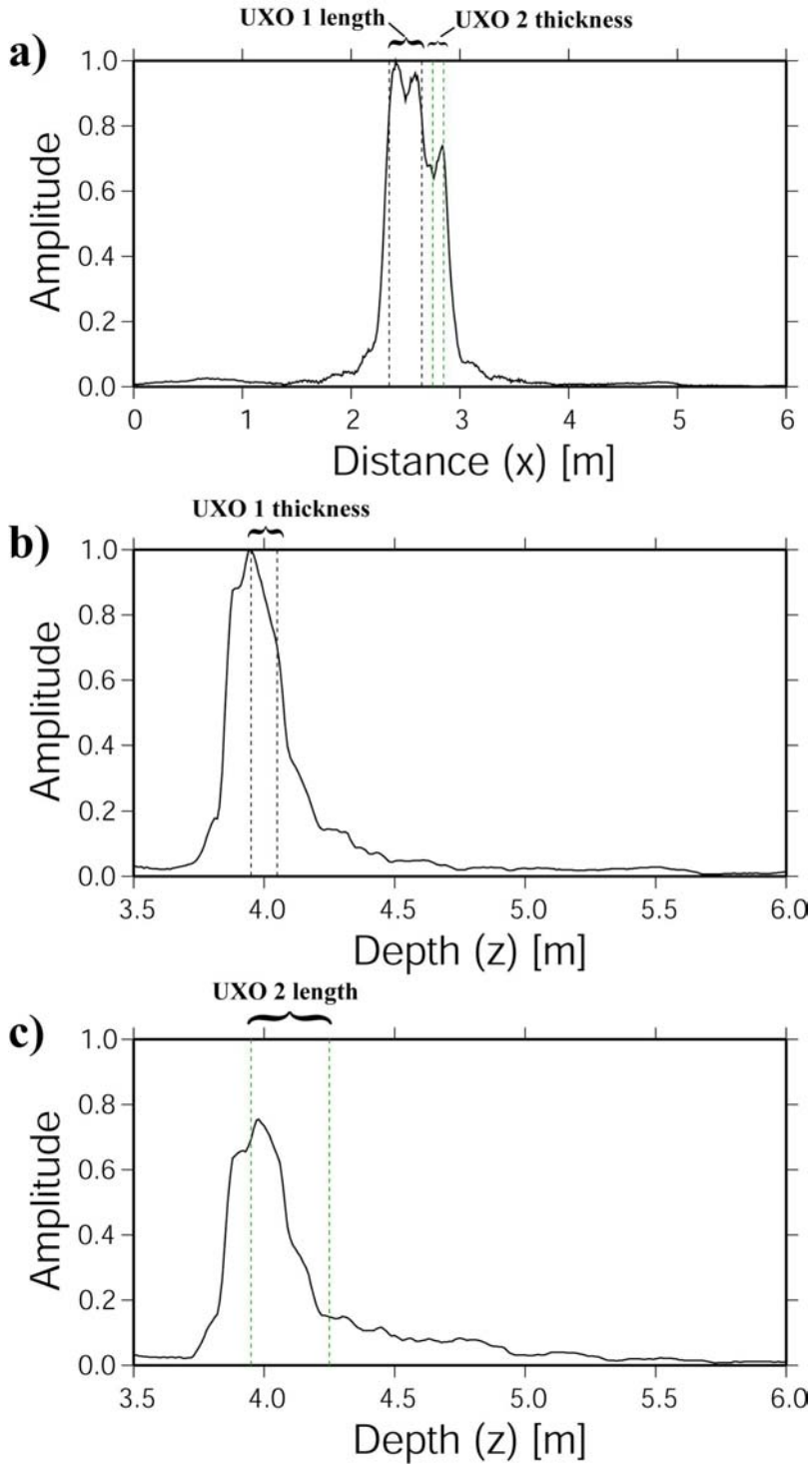

Figure 23: Cross sections of normalized amplitudes through the UXO signature in Figure 22. Colored dashed lines refer to the color-coding of UXO in Figures 20 and 22. **a)** Cross section in x-direction. **b)** Cross section in z-direction through UXO 1. **c)** Cross section in z-direction through UXO 2.

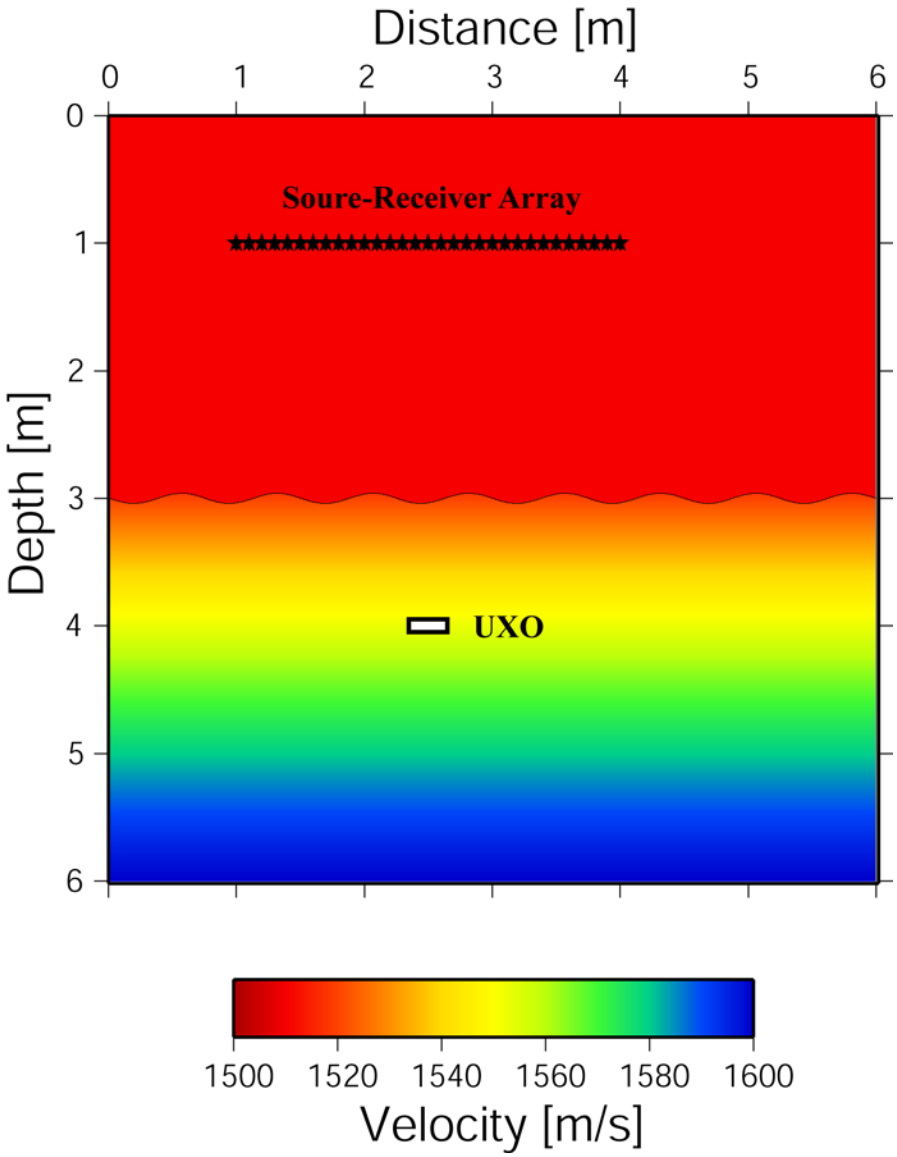

Figure 24: Same velocity model as in Figure 2, with the difference of a rippled seafloor.

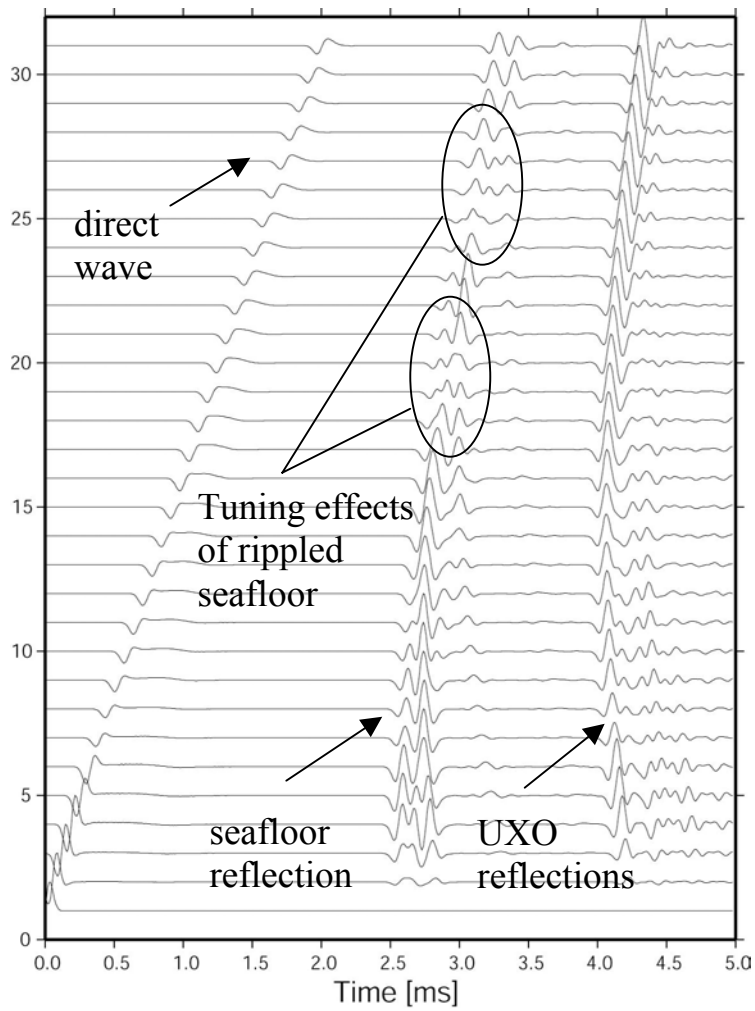

Figure 25: Seismic waveforms generated by the shot at x = 1m and z = 1 m and recorded by the receiver array with the model shown in Figure 24. Tuning effects can be seen in the signals reflected by the rippled seafloor.

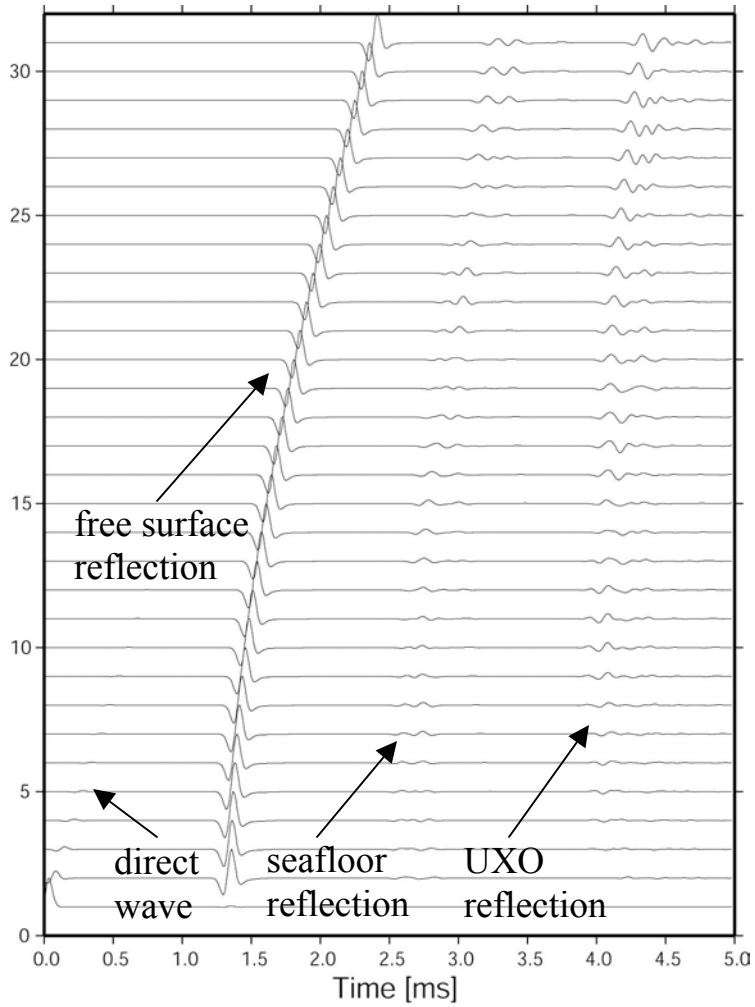

Figure 26: Seismic waveforms generated by the shot at x = 1m and z = 1 m and recorded by the receiver array, calculated for the model in Figure 24 with a free surface boundary condition.

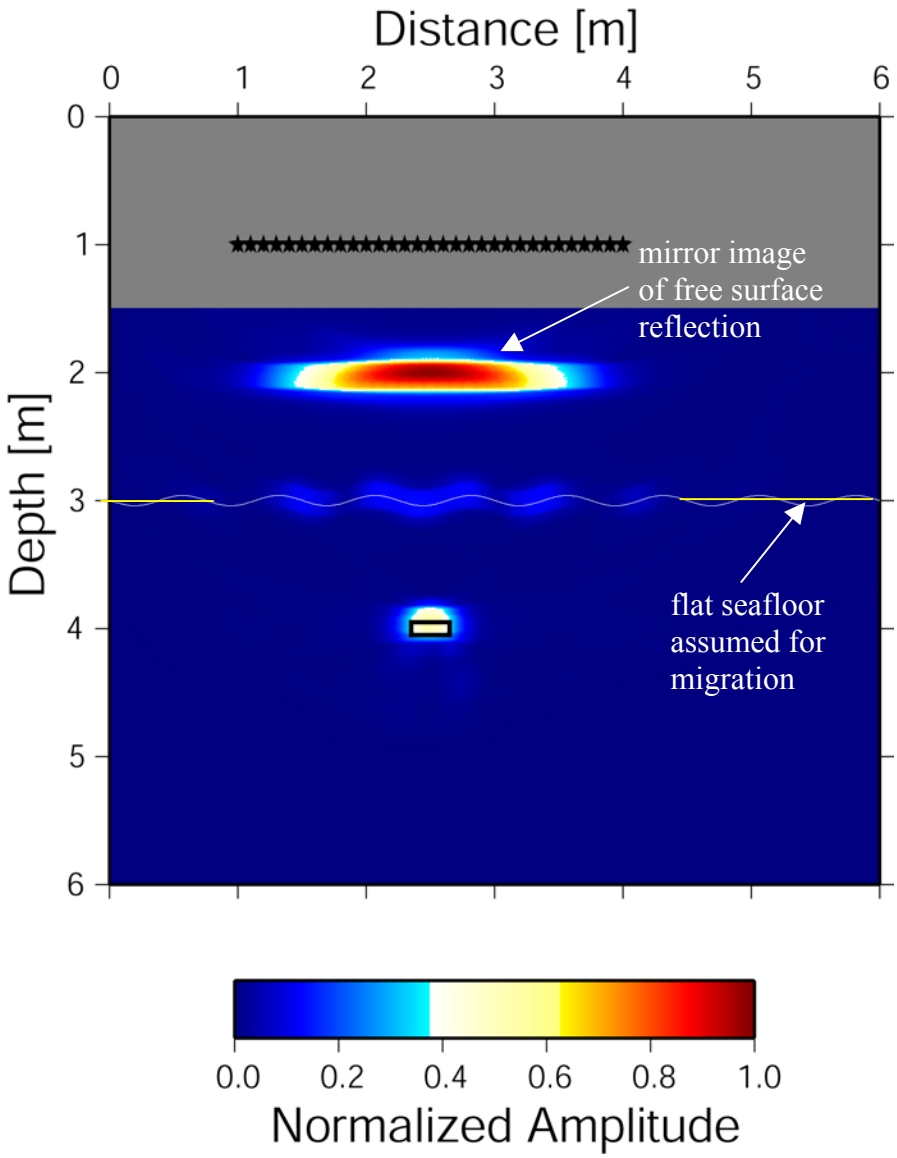

Figure 27: Normalized amplitude map of migrated waveforms recorded by the 31 sources and 31 receivers in the array. The migration was based on a velocity model with a flat seafloor and was carried out over a depth interval from 1.5 m to 6.0 m.

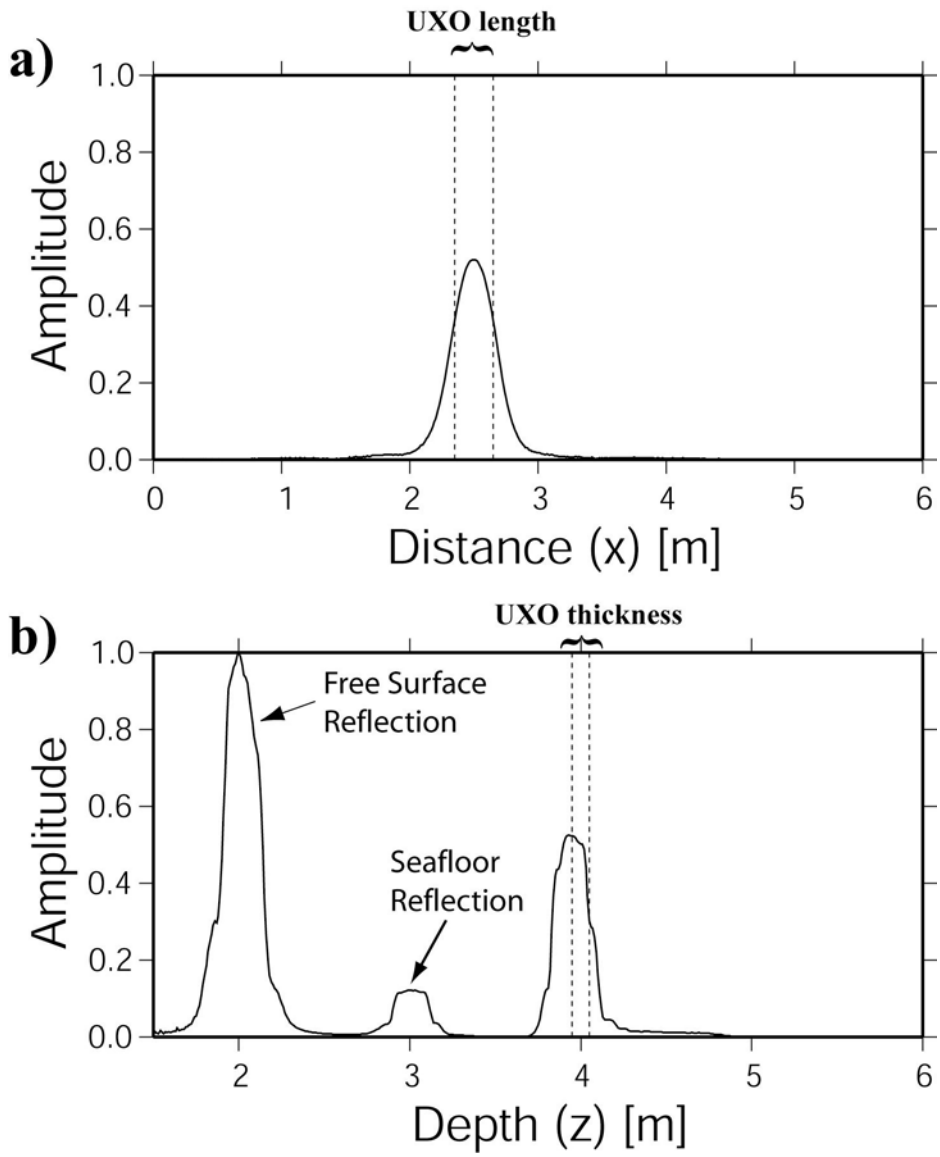

Figure 28: Cross sections of normalized amplitudes through the UXO signature in Figure 27. **a)** Cross section in x-direction. **b)** Cross section in z-direction.

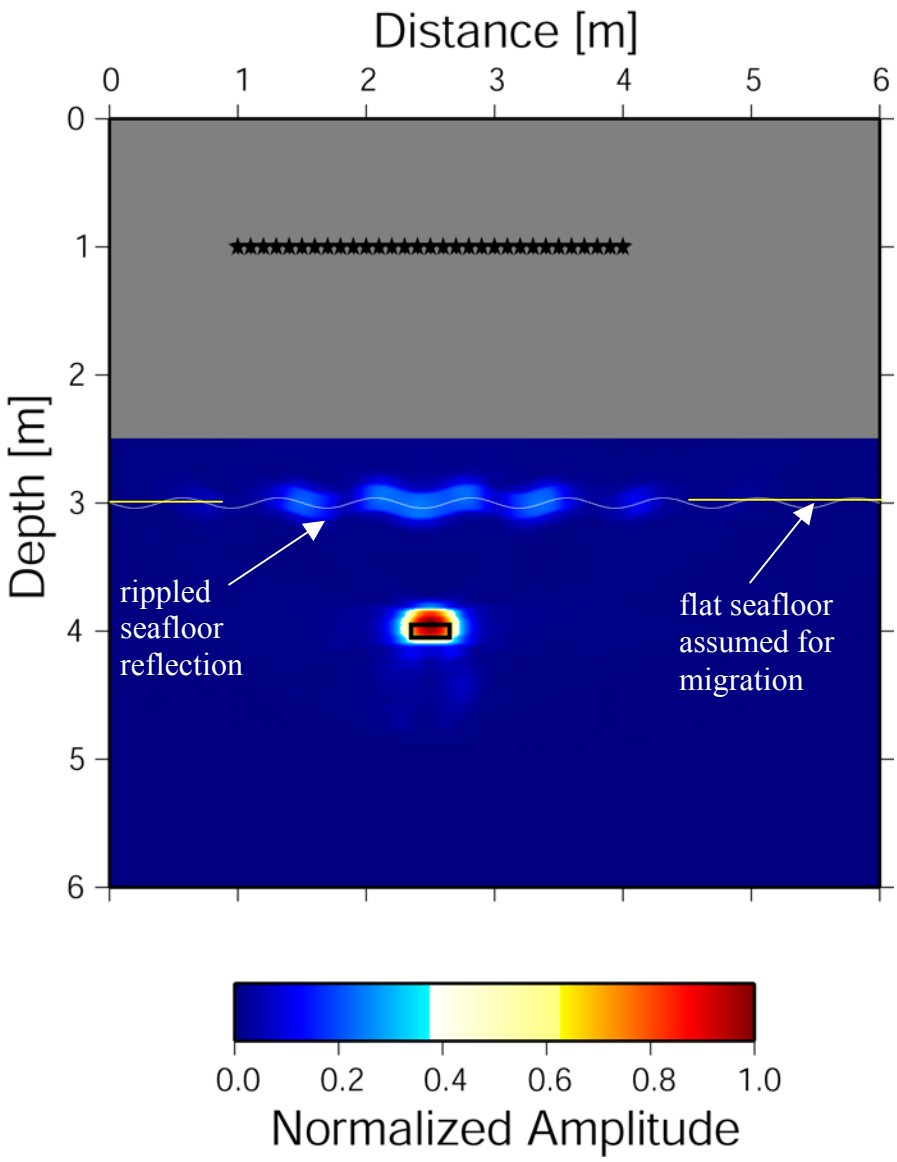

Figure 29: Same as Figure 27, with the exception that the migration was performed between 2.5 m and 6.0 depth.

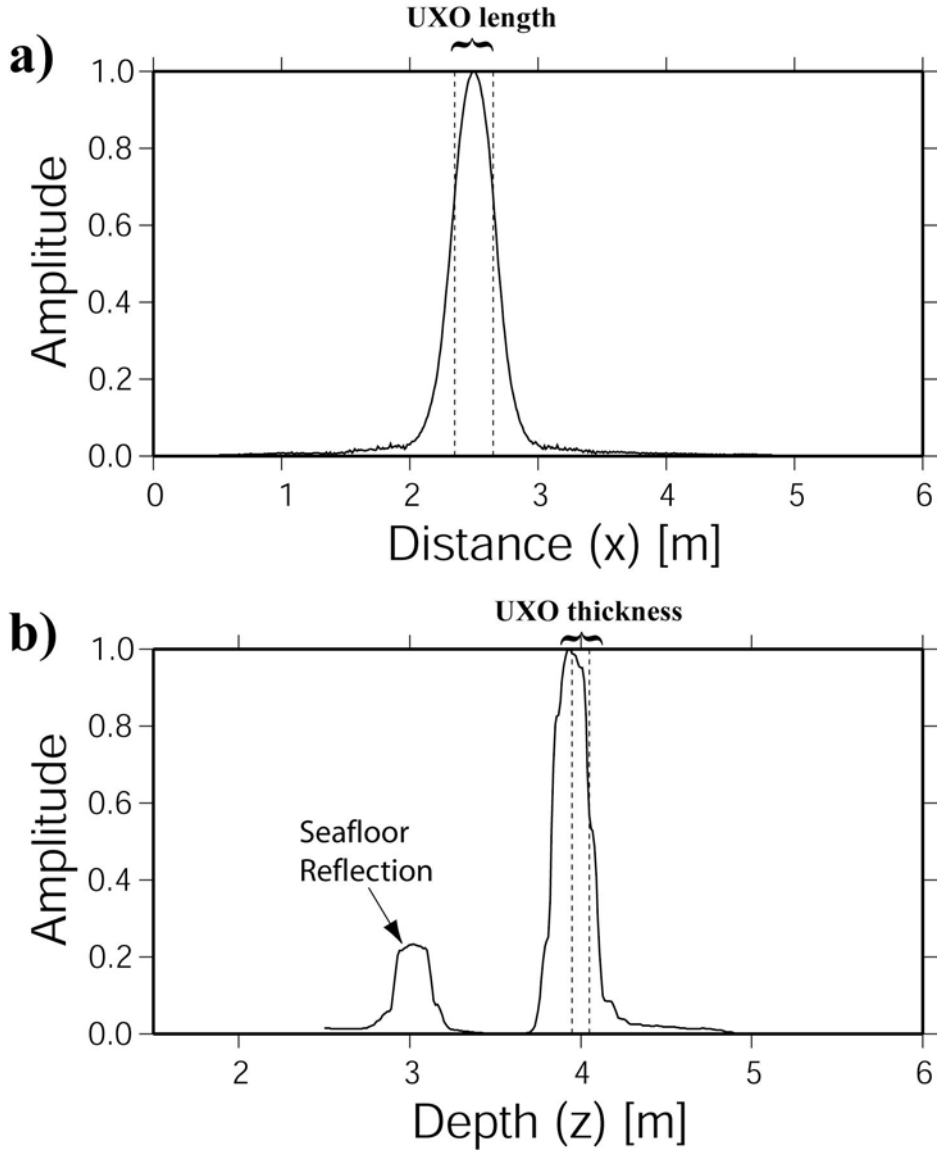

Figure 30: Cross sections of normalized amplitudes through the UXO signature in Figure 29. **a)** Cross section in x-direction.
b) Cross section in z-direction.

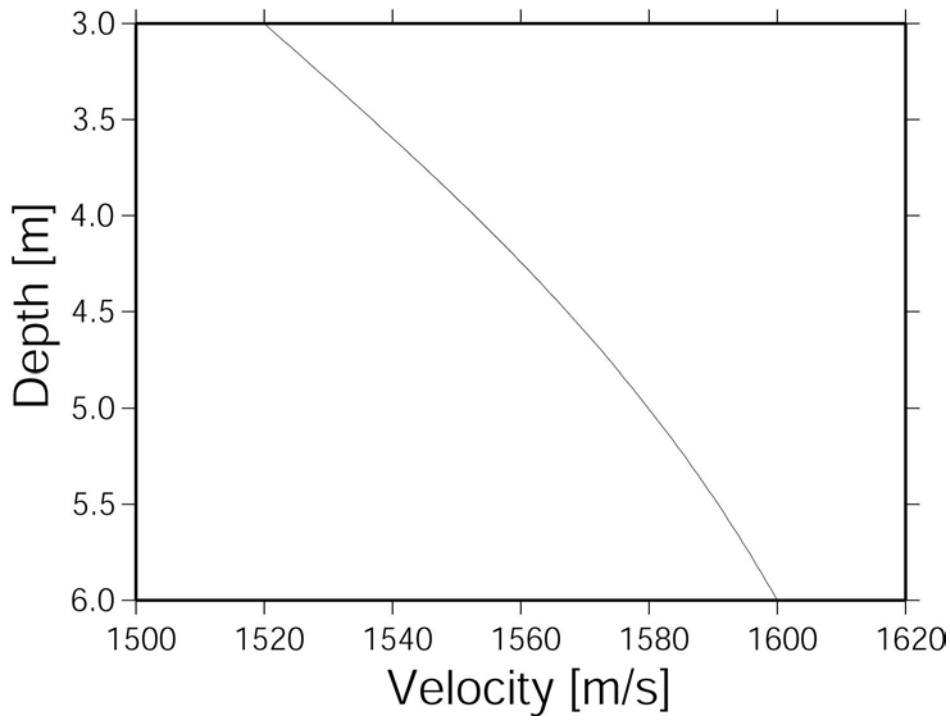

Figure 31: Velocity gradient of the sedimentary layer used throughout the finite difference models.

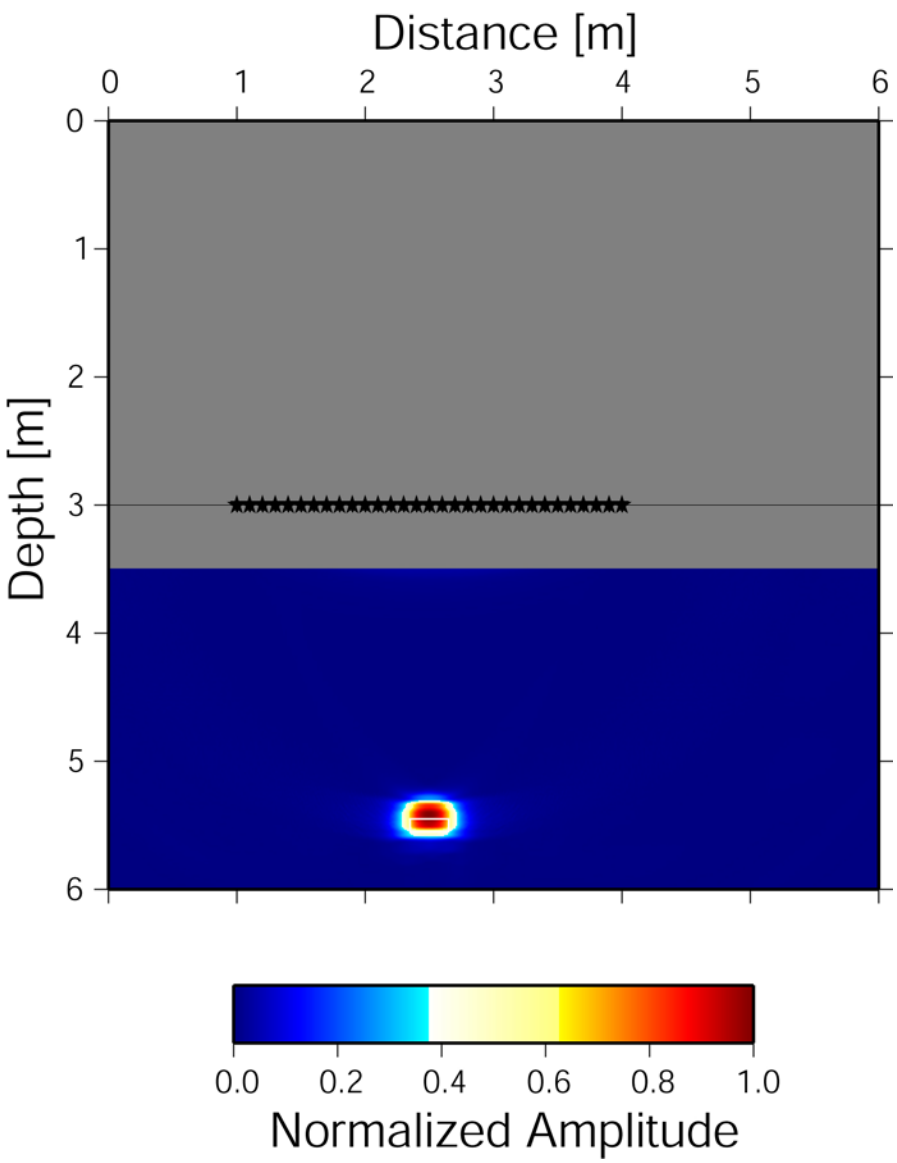

Figure 32: Normalized amplitude map of migrated waveforms recorded by the 31 sources and 31 receivers in the seafloor array for a UXO buried deeper in the sediments. The migration was carried out over a depth interval between 3.5 m and 6.0 m.

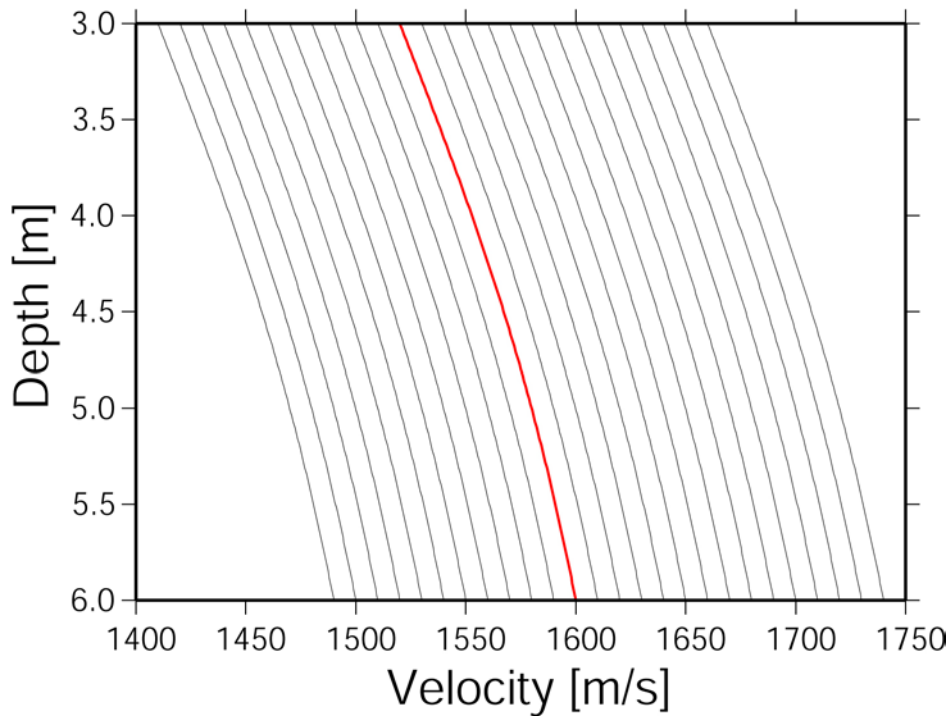

Figure 33: Velocity gradients of the sedimentary layer tested for the best migration result. The red line represents the correct gradient used during the finite difference calculations.

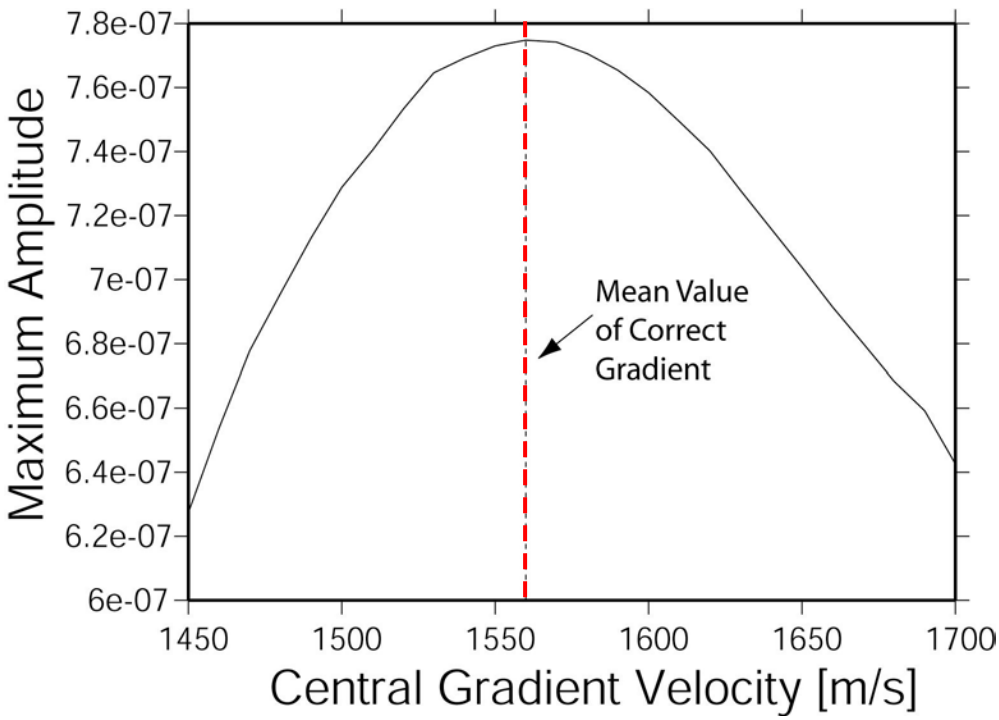

Figure 34: Result of the velocity inversion based on the gradients in Figure 33. The velocity values on the abscissa are mean values of the end points of each gradient in Figure 33. The dashed line indicates the mean value of the correct gradient.

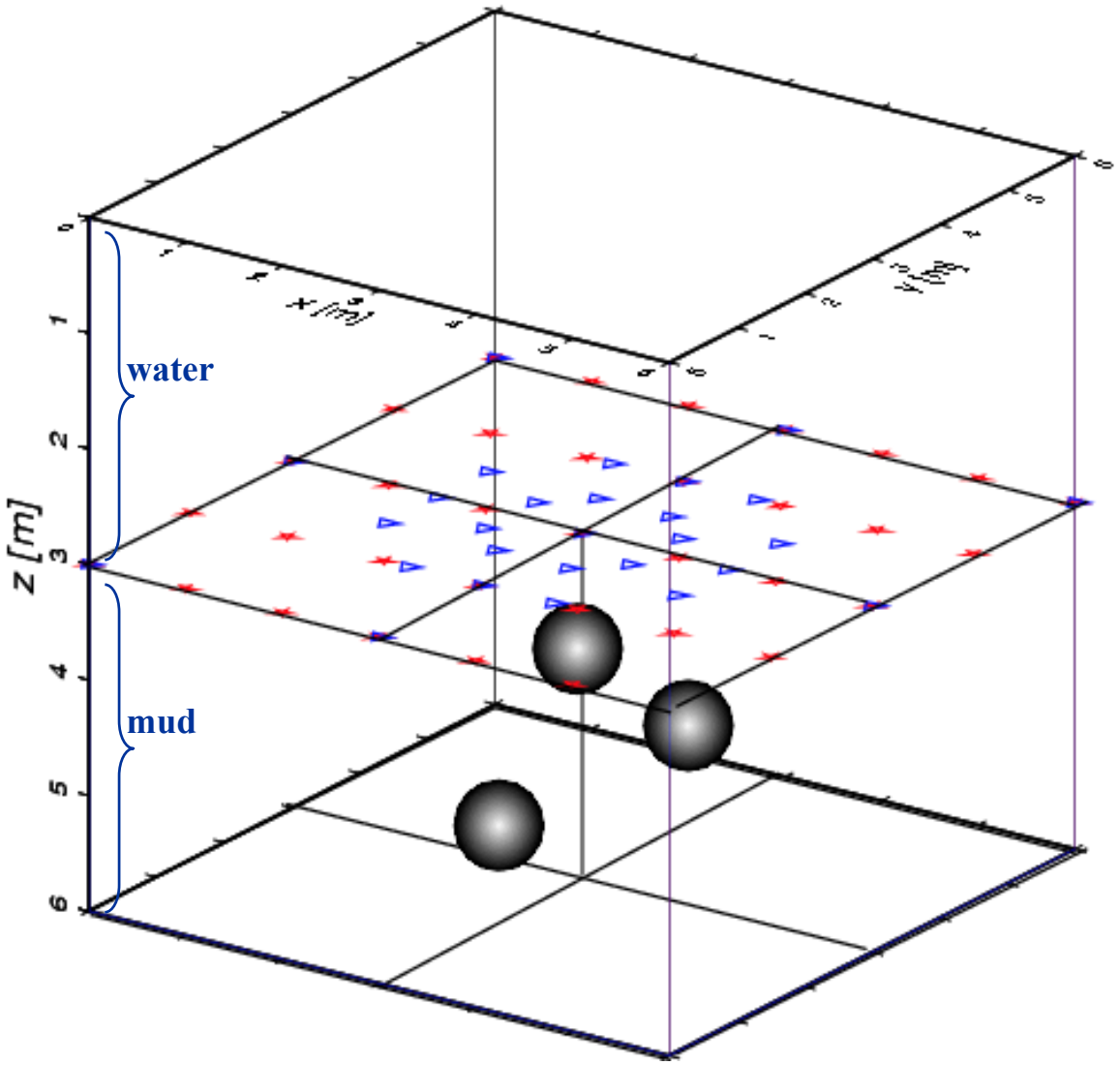

Figure 35: Geometry of the 3-D modeling task. The model has a length of 6 m on each side, with the vertical divided into a 3 m water layer above a 3 m thick sedimentary layer. The three UXO are located along two vertical slices in xz- and yz-direction. The source-receiver array is located along the seafloor with the sources indicated by the red stars, while the receivers are denoted by blue triangles.

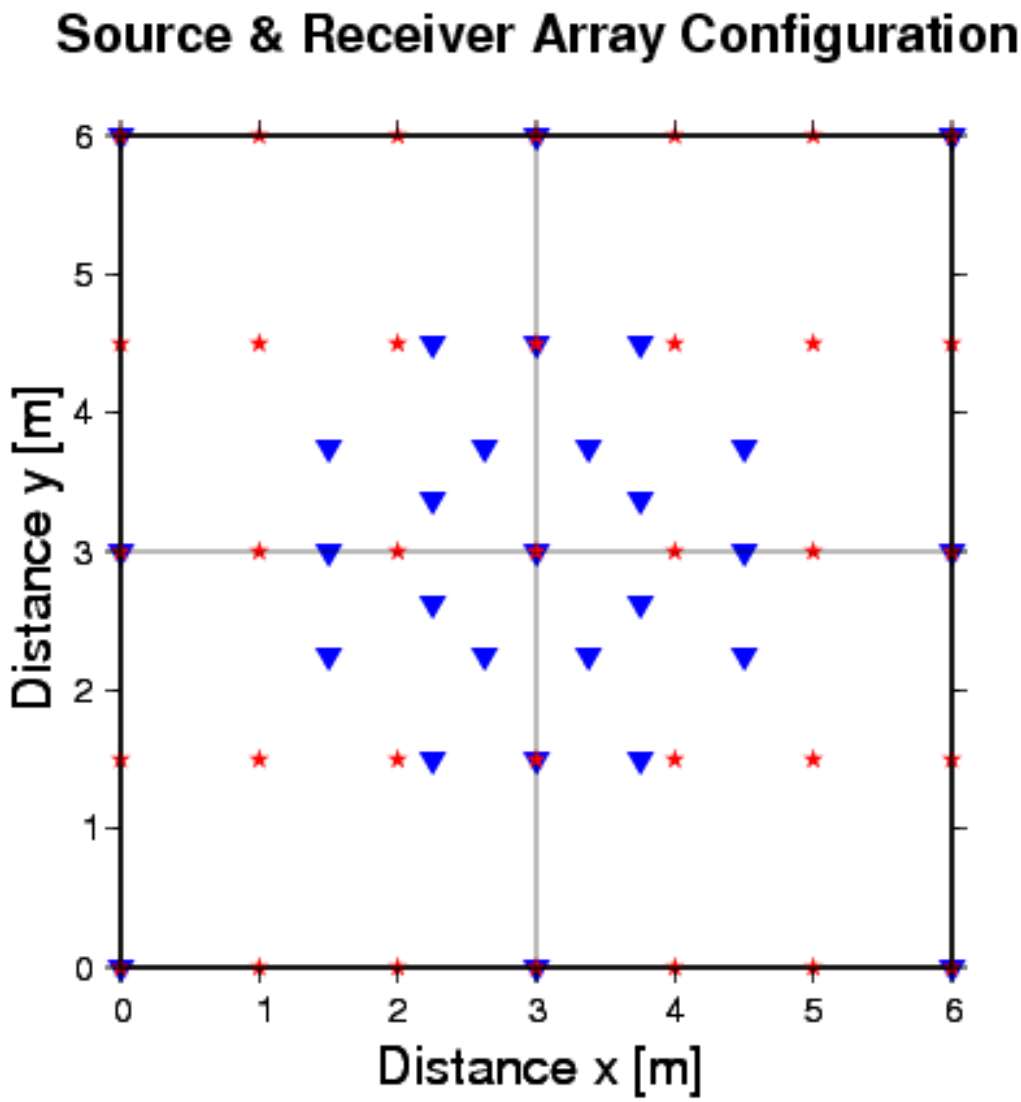

Figure 36: 2-D view of the source-receiver array shown in Figure 35.

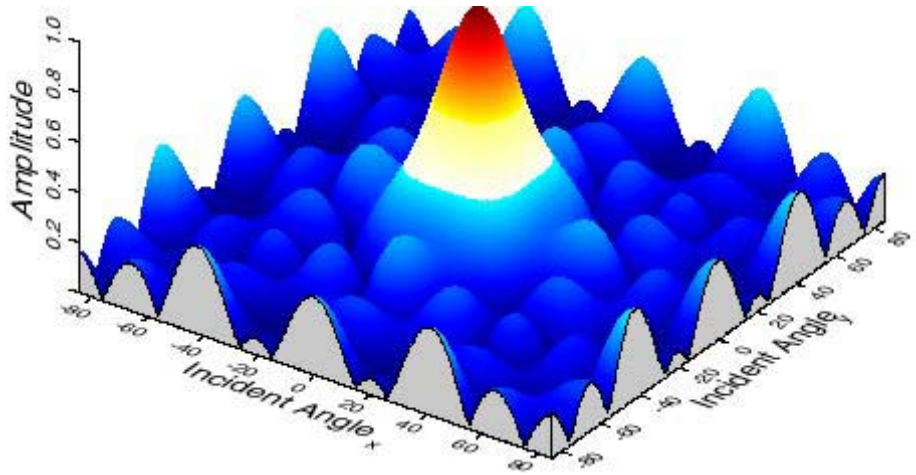

Figure 37: Array response of the receiver configuration in Figure 36 for a 1kHz wave. Focus is vertically down.

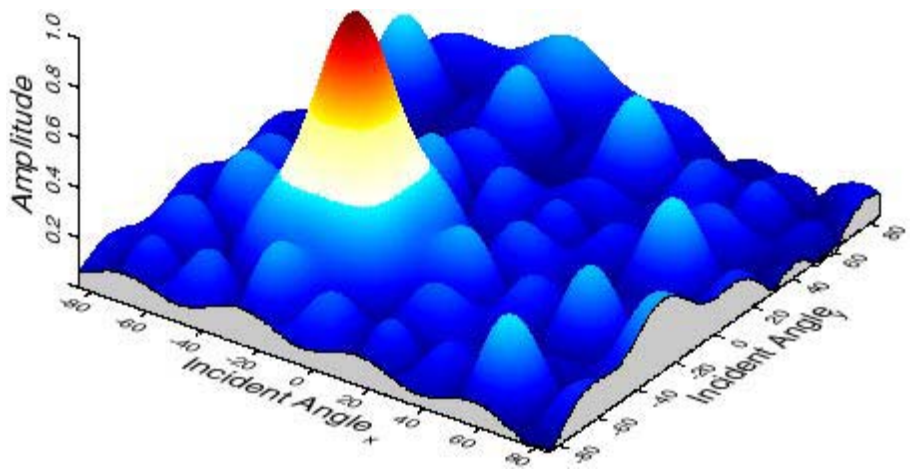

Figure 38: Array response of the receiver configuration in Figure 36 for a 1kHz wave. Focus is at $i_x = -35^o$ and $i_y = -35^o$.

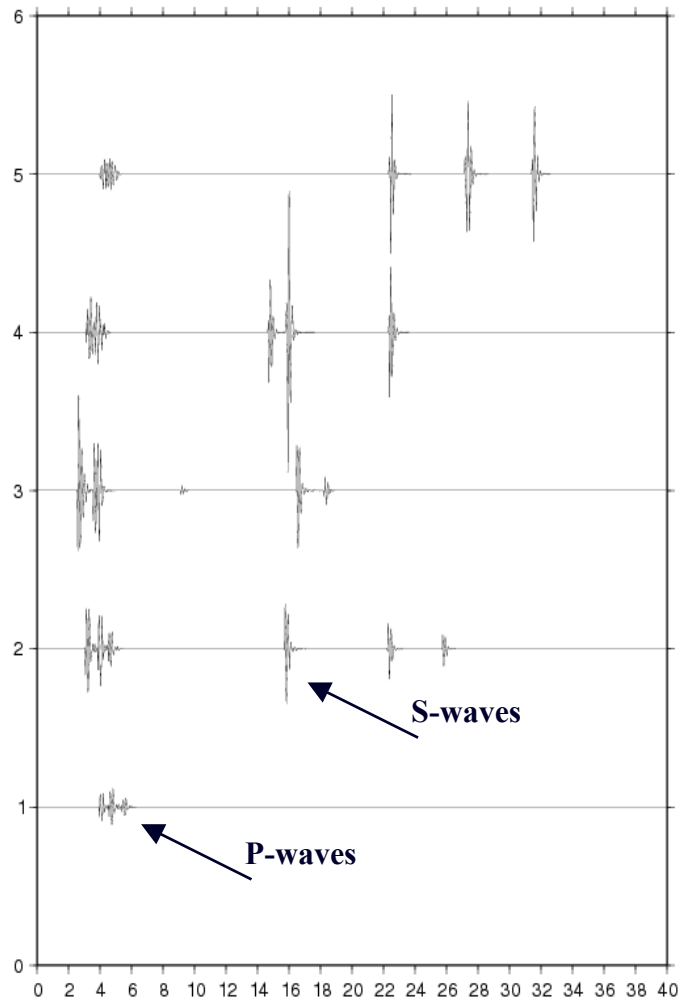

Figure 39: Seismic waveforms generated by the shot located at x=0 m, y=3 m, and z=3 m, while the receivers are located at y=3 m between x=0 m and 6 m. The data were generated with a 5kHz source signal.

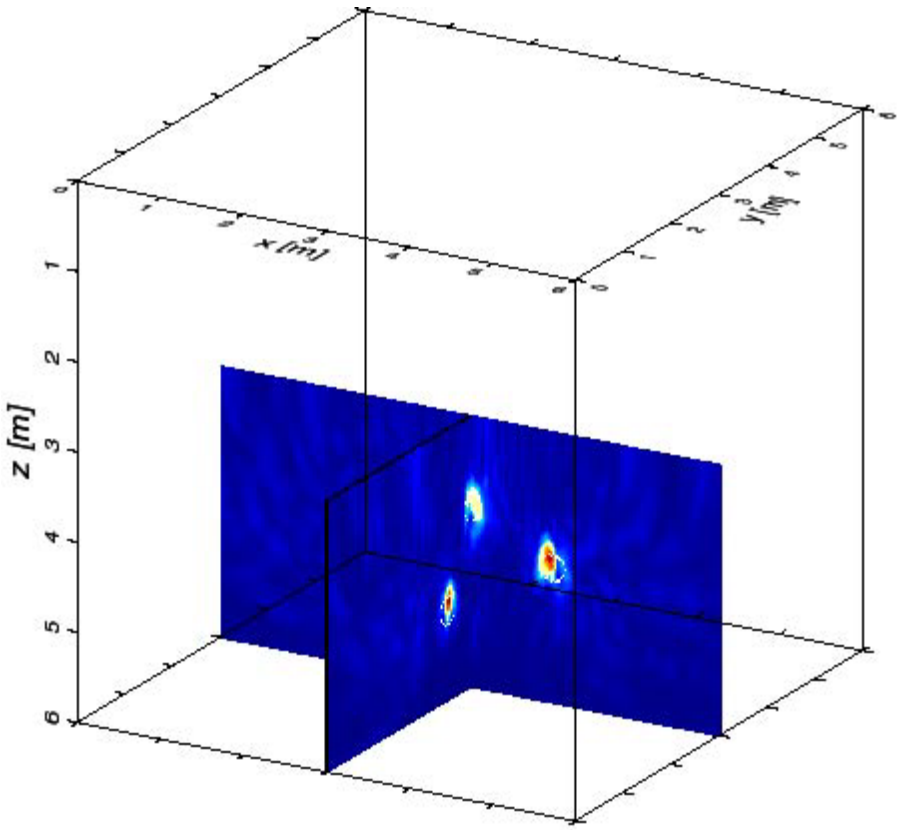

Figure 40: Normalized amplitude map of migrated waveforms recorded by the 2-D array in Figure 35. The migration was carried out over a depth interval from 3 m to 6 m. The fence diagram displays the part of the data cube that crosses the UXO locations. The white circles outline the locations of the UXO.

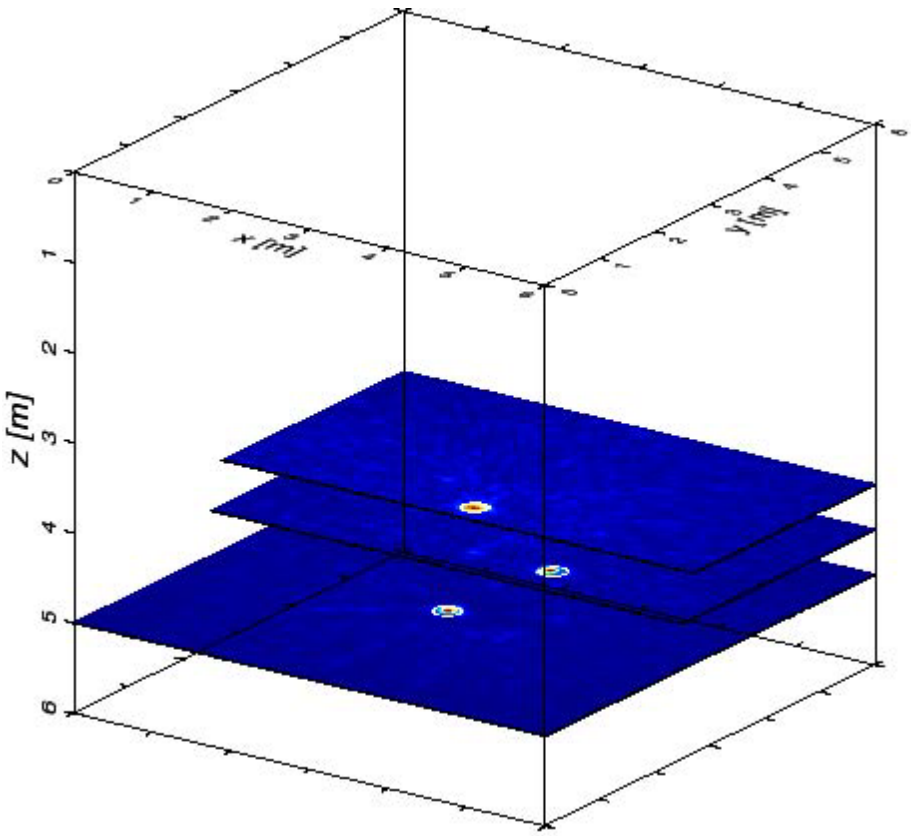

Figure 41: Normalized amplitude map of migrated waveforms recorded by the 2-D array in Figure 35. The migration was carried out over a depth interval from 3 m to 6 m. The horizontal slices display the parts of the data cube that cross the UXO locations. The white circles outline the locations of the UXO.

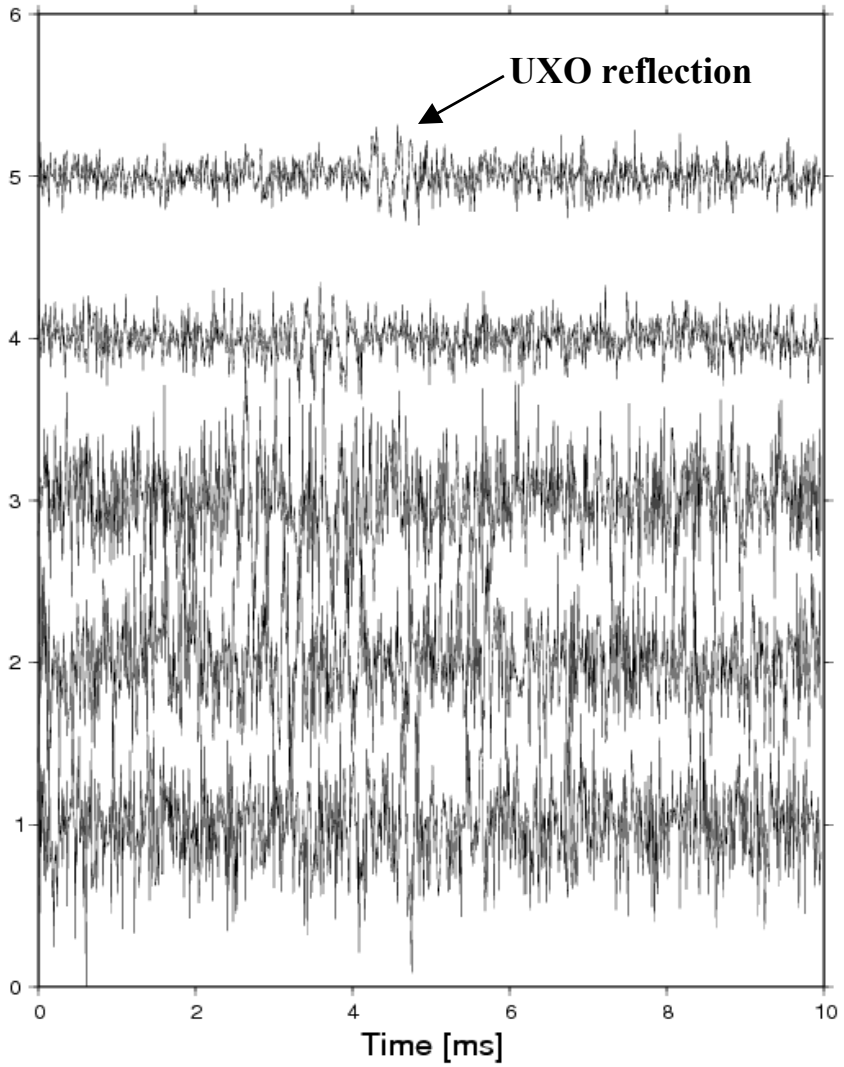

Figure 42: Same as Figure 39 with the addition of 50% Gaussian distributed noise.

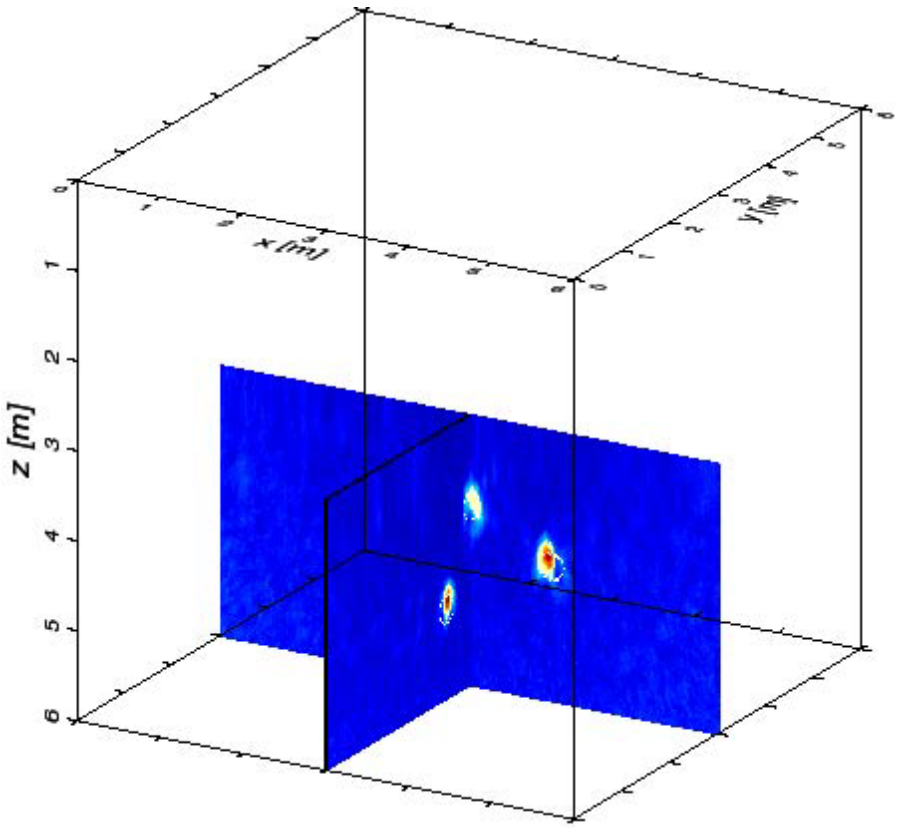

Figure 43: Normalized amplitude map of the migrated waveforms as shown in Figure 42. The migration was carried out over a depth interval from 3 m to 6 m. The fence diagram displays the part of the data cube that crosses the UXO locations. The white circles outline the locations of the UXO.

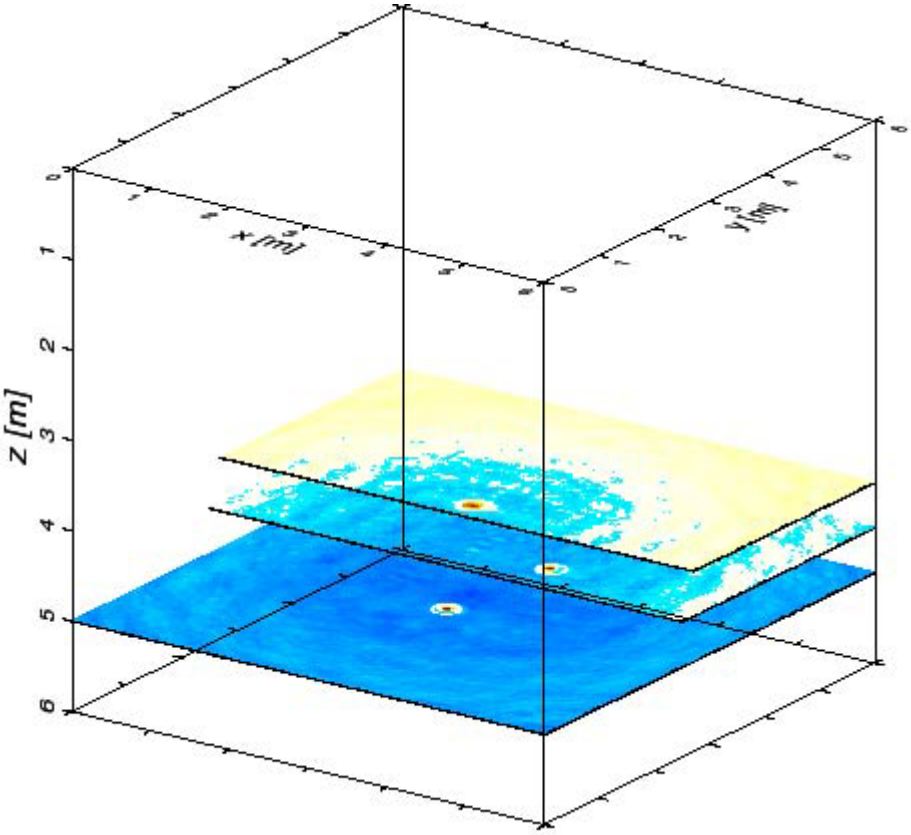

Figure 44: Normalized amplitude map of the migrated waveforms as shown in Figure 42. The migration was carried out over a depth interval from 3 m to 6 m. The horizontal slices display the parts of the data cube that cross the UXO locations. The white circles outline the locations of the UXO.

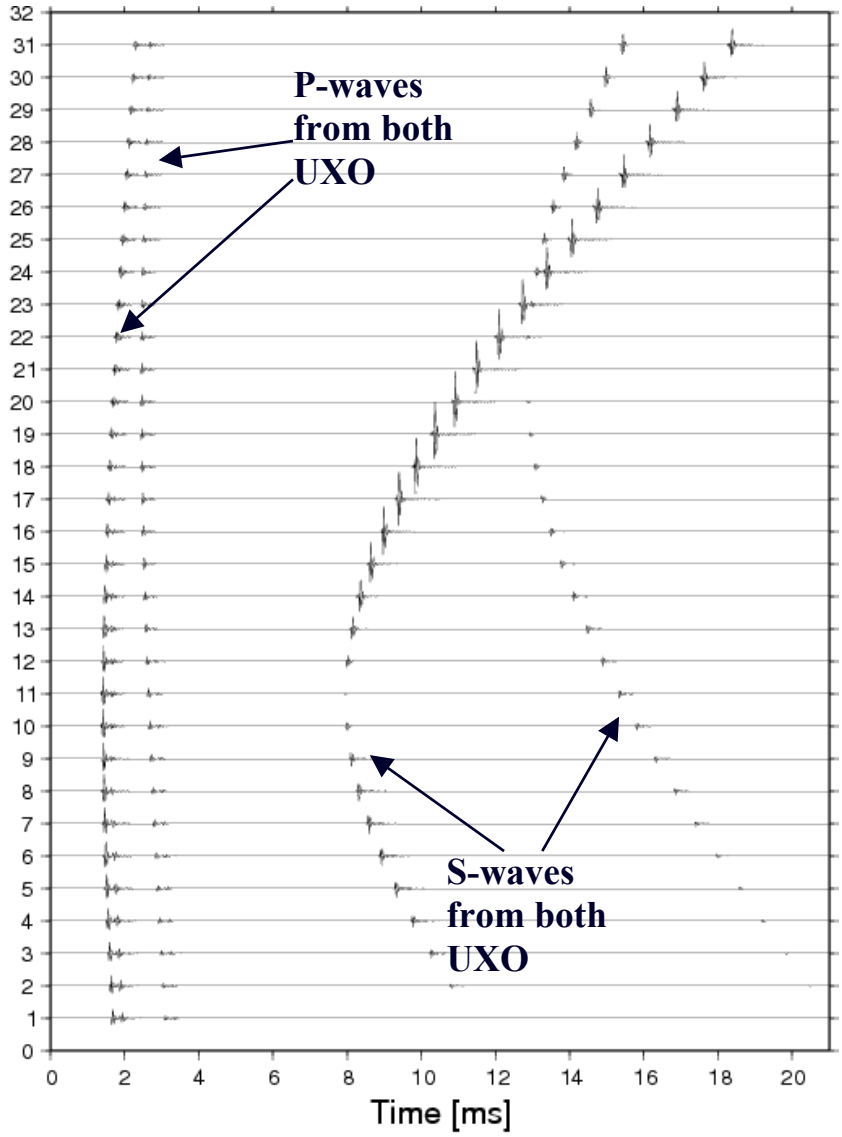

Figure 45: Seismic waveforms generated by the 1-D source-receiver array, presented in Figure 46. The waveforms were generated by two spherical shaped UXO located beneath the array. The frequency of the source pulse was 15 kHz.

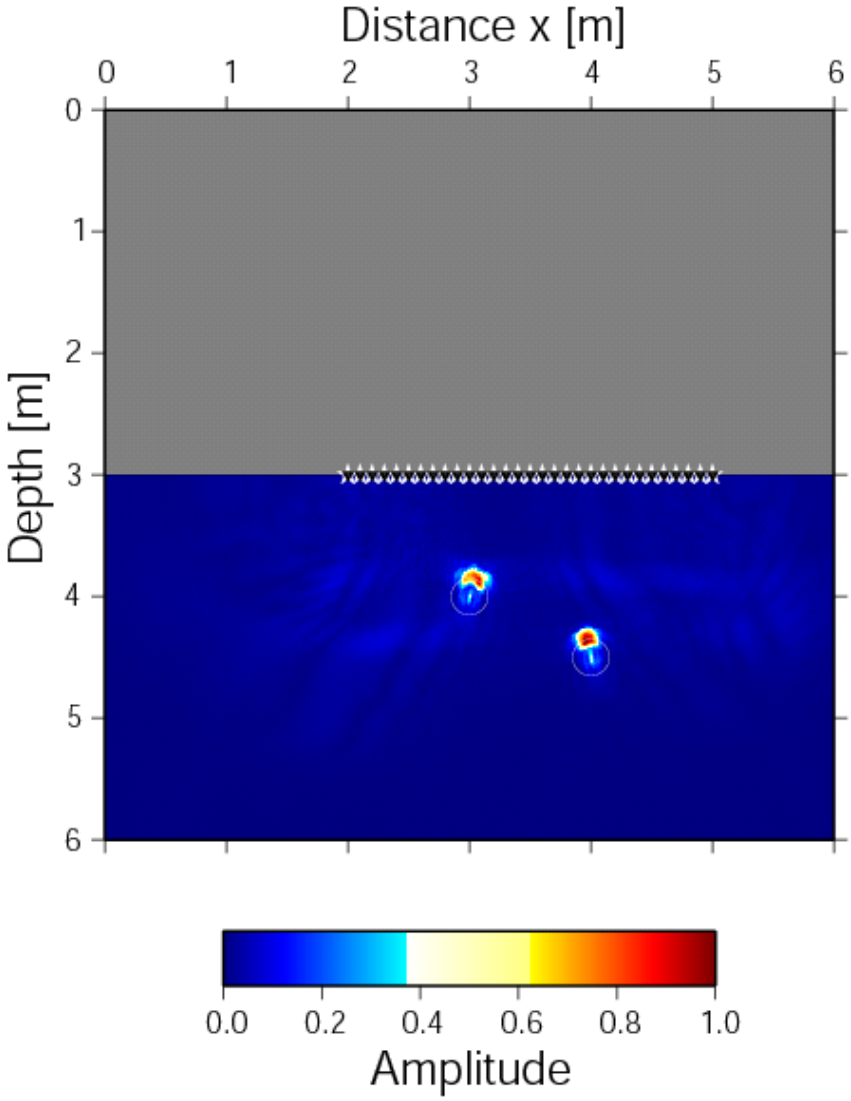

Figure 46: Normalized amplitude map of the migrated P-waves shown in Figure 45. The migration was carried out over a depth interval from 3 m to 6 m. The white circles outline the locations of the UXO.

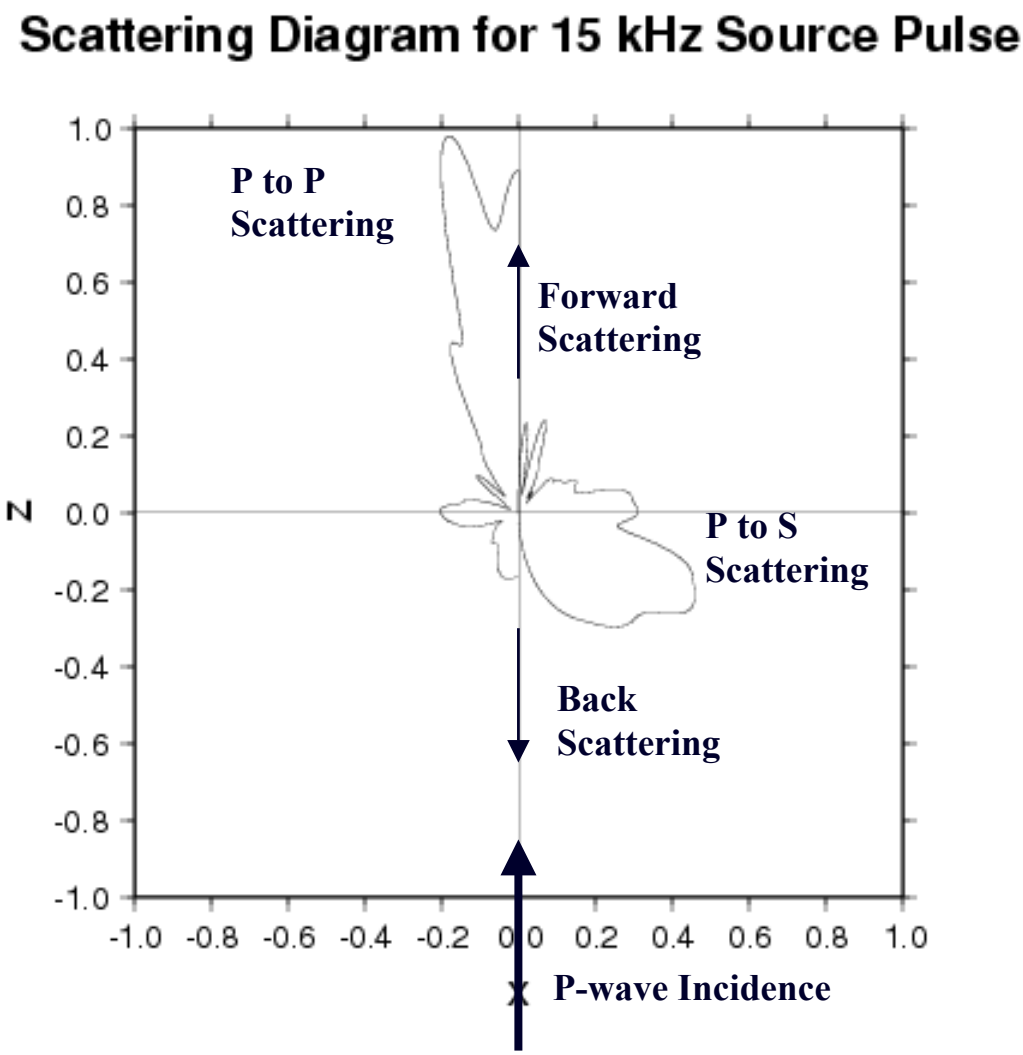

Figure 47: Scattering diagram for a 15 kHz P-wave incident from below. The left and right part of the diagram characterize, respectively, P-to-P and P-to-S scattering, while the positive and negative z-axis denotes forward and backward scattering.

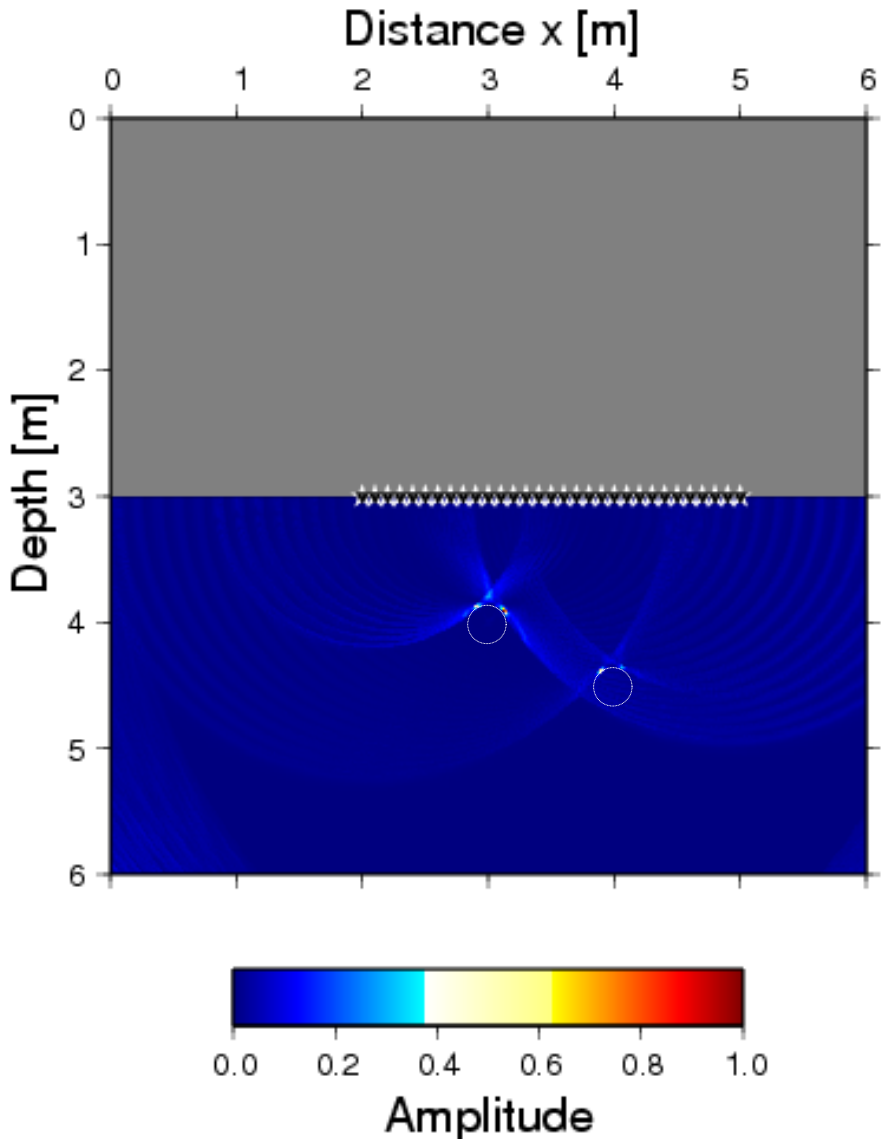

Figure 48: Normalized amplitude map of the migrated S-waves shown in Figure 45. The migration was carried out over a depth interval from 3 m to 6 m. The white circles outline the locations of the UXO.

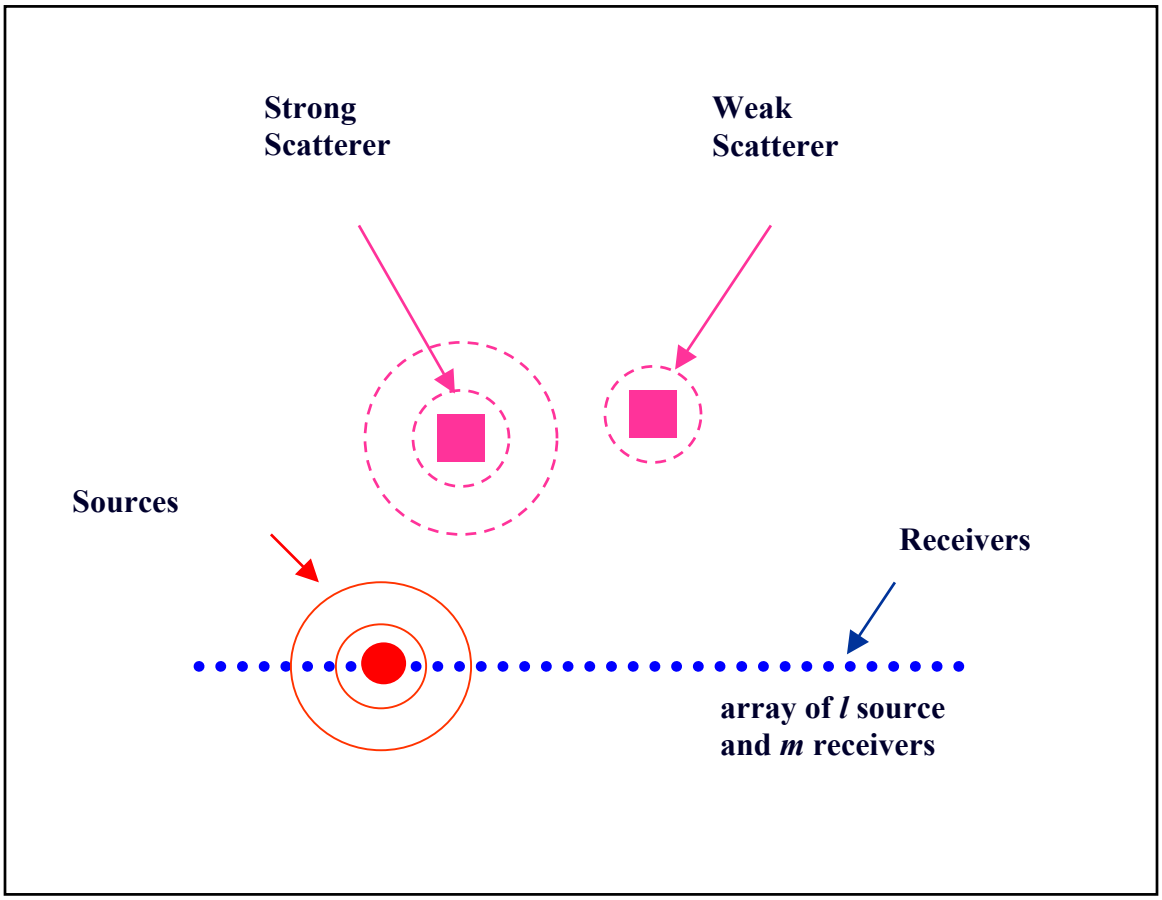

Figure 49: Schematic geometry of a source and receiver array with two scatterers of different strength.

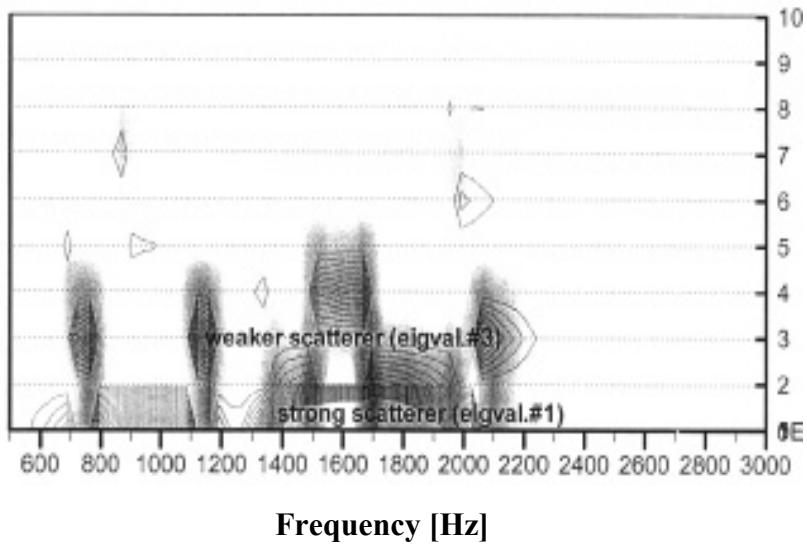

Figure 50: Decomposition of the eigenvalues of the problem in Figure 49, as a function of frequency. The eigenvalues #1 and #3 correspond to the stronger and weaker scatterers, respectively.

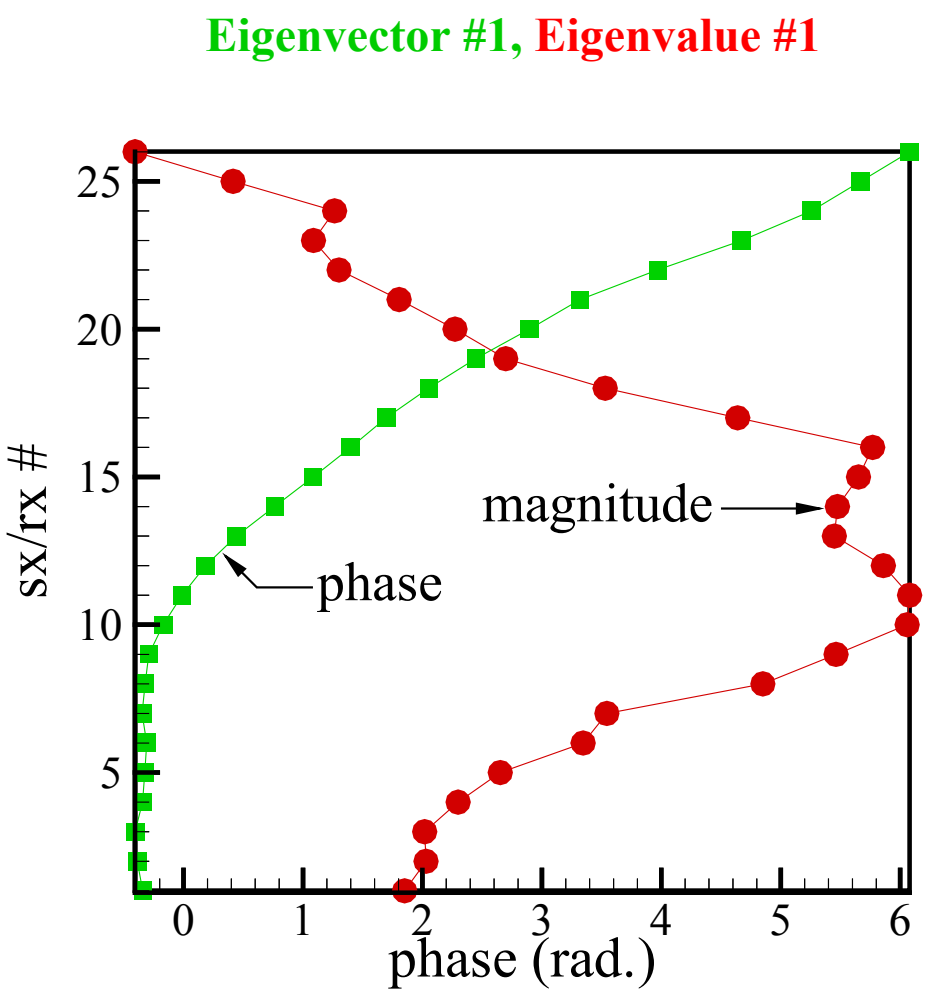

Figure 51: The eigenvectors and eigenvalues of the decomposed transfer matrix are used to phase the array and apply the correct source strength to focus on specific targets in the medium.

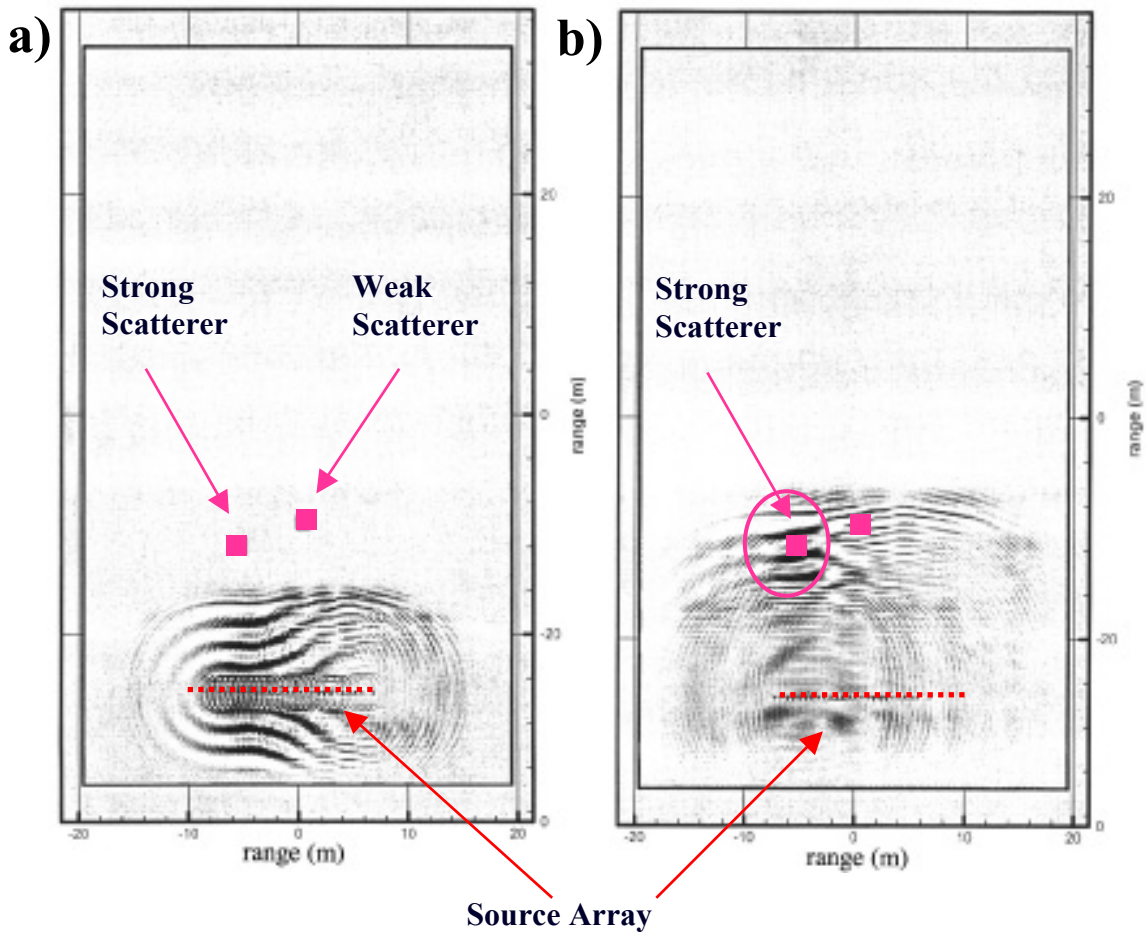

Figure 52: Time snapshots of wavefronts steered by the source array to focus onto the strong scatterer in the medium. The dark shaded areas represent the amplitudes of the waves as they propagate through the medium in time.

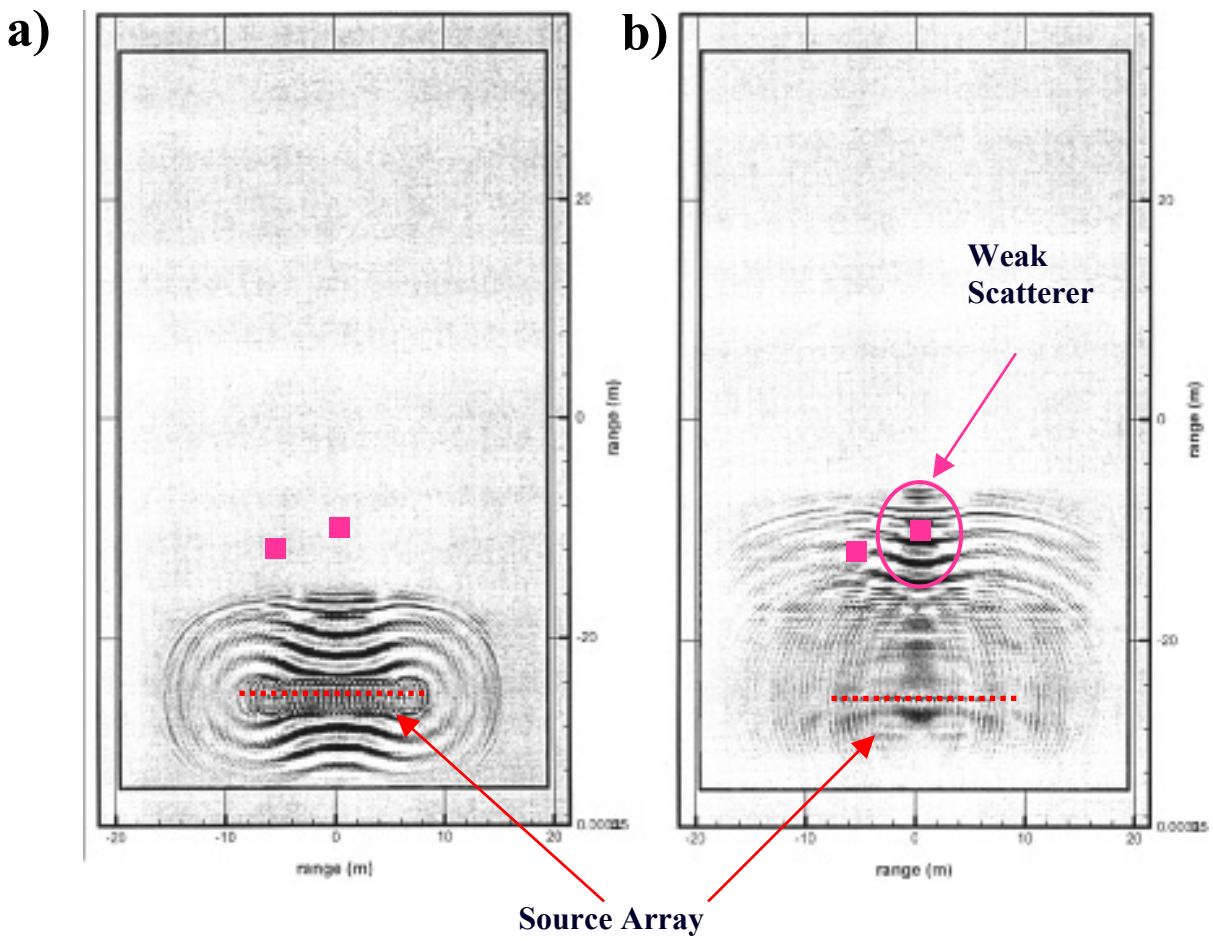

Figure 53: Time snapshots of wavefronts steered by the source array to focus onto the weak scatterer in the medium. The dark shaded areas represent the amplitudes of the waves as they propagate through the medium in time.